ELSEVIER

Chemical Engineering Science 61 (2006) 3105–3128

Chemical Engineering Science

www.elsevier.com/locate/ces

Fuzzy diagnosis method for control systems with coupled feed forward and feedback loops

Jung Yang Chen, Chuei-Tin Chang*

Department of Chemical Engineering, National Cheng Kung University, Tainan, Taiwan 70101, ROC

Received 14 March 2005; received in revised form 14 September 2005; accepted 29 November 2005
Available online 24 January 2006

Abstract

By considering the fault propagation behaviors in control systems with coupled feed forward and feedback loops, a fuzzy-logic-based fault diagnosis strategy has been developed in the present work. The proposed methods can be implemented in two stages. In the off-line preparation stage, the root causes of a system hazard are identified by determining the minimal cut sets of the corresponding fault tree. The occurrence order of observable disturbances caused by each fault origin is derived from the system digraph. All possible patterns of the on-line symptoms and their evolution sequences can then be deduced accordingly. These sequences are used as the basis for constructing a two-layer fuzzy inference system. In the next on-line implementation stage, the occurrence indices of the root causes are computed with the IF–THEN rules embedded in the inference engine using the real-time measurement data. Numerical simulation studies have been carried out to demonstrate the feasibility of the proposed approach.

Keywords: Fault diagnosis; Fuzzy logic; Systems engineering; Safety; Process control; Dynamic simulation

1. Introduction

As a result of increasing complexity in the modern chemical processes, the development of computer-aided on-line fault diagnosis techniques has become an important research issue for enhancing operation safety in industrial plants. Although a wide variety of approaches have been proposed in the past, e.g., state estimator (Chang and Chen, 1995), expert system (Petti et al., 1990), neural network (Hoskins et al., 1991), signed directed graph (SDG) (Iri et al., 1979; Kramer and Palowitch, 1987; Shiozaki et al., 1985; Tsunge et al., 1985), etc., none of them are mature enough for practical implementation. In this work, fault diagnosis is performed on the basis of an alternative tool, i.e., the fault tree. Fault tree analysis (FTA) is in fact a well-established off-line hazard assessment technique. One of the most popular model used in the development of algorithms for automating FTA is perhaps the digraph. The digraph-based fault-tree synthesis strategy was first proposed by Lapp and Powers (1977). Numerous other studies concerning its applications and modifications have been published in the literature (Allen, 1984; Allen and Rao, 1980; Andrews and Brennan, 1990; Andrews and Morgan, 1986; Chamow, 1978; Cummings et al., 1983; Lambert, 1979; Lapp and Powers, 1979; Shaeiwitz et al., 1977). Essentially, a digraph provides an intermediate step which gives explicit causal relationships between the process variables, human errors and equipment failures, from which the fault trees can be constructed accordingly. In particular, a set of generalized fault-tree structures (operators) corresponding to various digraph configurations were developed for control systems with coupled loops, e.g., Lapp and Powers (1977), Chang and Hwang (1992), Chang and Hwang (1994), Chang et al. (1994), and Ju et al. (2003, 2004).

Ulerich and Powers (1988) reported the first attempt to apply fault tree on-line for fault diagnosis purpose. The most significant advantage of their method is that the candidates of fault identification are restricted to only the causes of one or more given top events and, consequently, the diagnosis

Abbreviations: FIS, fuzzy inference system; FPP, fault propagation path; PES, pattern evolution sequence; SDG, signed directed graph; SOO, symptom occurrence order

* Corresponding author. Tel.: +886 6 275 7575ext.62663; fax: +886 6 234 4496.
E-mail address: ctchang@mail.ncku.edu.tw (C.-T. Chang).

0009-2509/$ - see front matter © 2006 Elsevier Ltd. All rights reserved.
doi:10.1016/j.ces.2005.11.062

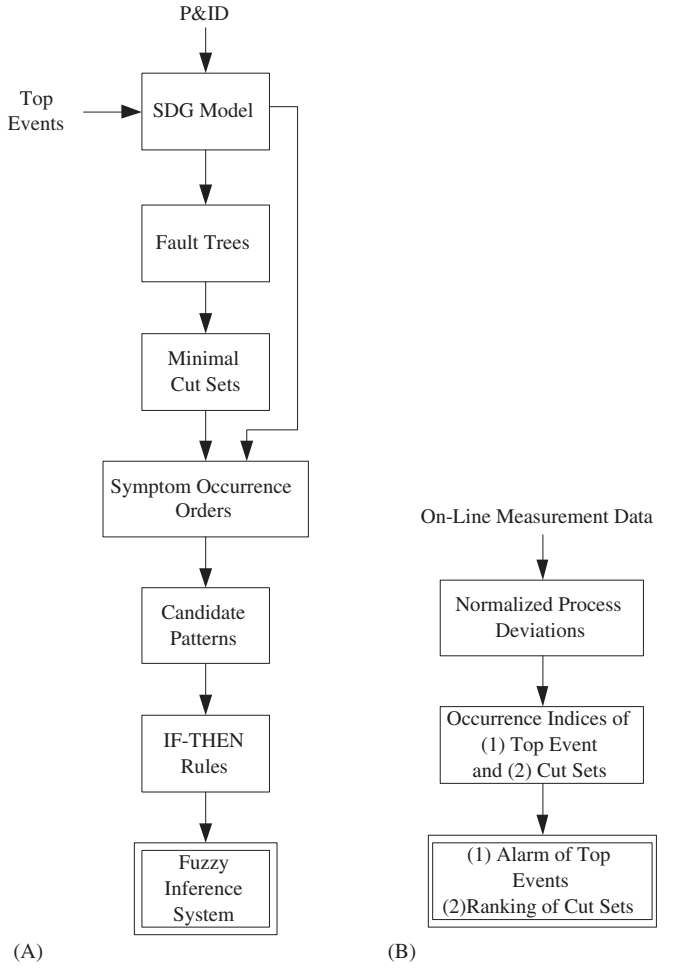

Fig. 1. The proposed fault diagnosis procedure: (A) off-line preparation stage (B) on-line implementation stage.

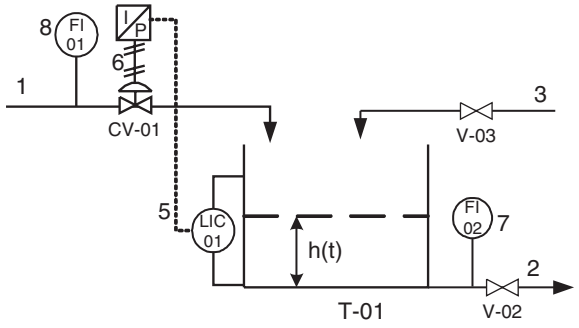

Fig. 2. A level control system.

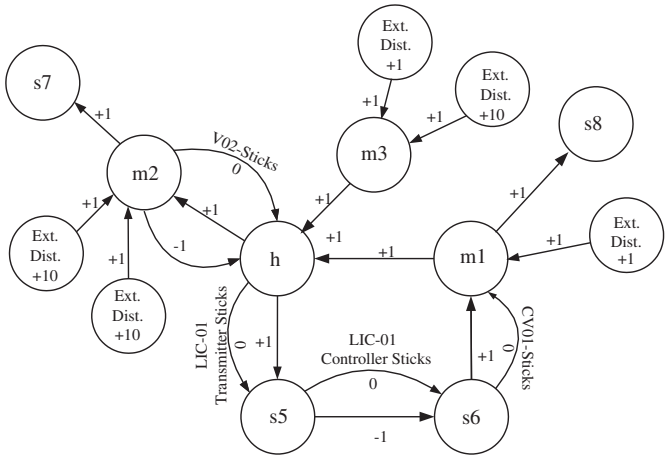

Fig. 3. Digraph model of level control system.

procedure can be greatly simplified. However, only a conceptual framework was proposed in this original study and, naturally, further improvements are required to facilitate application in a realistic environment. By incorporating the fault propagation patterns in a fuzzy inference system (FIS), Chang et al. (2002) and Chang and Chang (2003) developed a systematic fault diagnosis procedure on the basis of fault trees. This method was implemented in two stages according to the flowchart given in Fig. 1, i.e., (1) the off-line preparation stage and (2) the on-line implementation stage. In the former case, a SDG system model was first constructed and the fault trees corresponding to the given top events were then synthesized. The symptom occurrence order (SOO) caused by the basic events in each cut set can be easily determined with the SDG model. The candidate symptom patterns were then translated into a set of IF–THEN fuzzy inference rules for assessing the occurrence possibilities of fault origins. In the next stage, the on-line measurement data were normalized and then used as inputs to the FIS for computing all occurrence indices. This fault diagnosis strategy has been applied successfully to a number of loop-free processes (Chang et al., 2002) and also to systems with a single feedback control loop (Chang and Chang, 2003). In addition to the above studies, several other closely related works can also be found in the recent literature, e.g., Maurya et al. (2004), Tarifa and Scenna (2004) and Zhang et al. (2005). These authors utilized essentially the same tools, i.e., SDG and/or fuzzy logic, for fault diagnosis purpose, but took different approaches in their applications.

In reality, the SDG model of an industrial-size chemical process almost always contains tangled feed forward and feedback loops and thus the system dynamics could be much more

Table 1
Minimal cut sets of the fault tree in Fig. 4

MCS no.	Flow rate			CV-01 sticks	LIC-01 transmitter sticks	LIC-01 controller sticks
	m_1	m_2	m_3			
1		−10				
2			+10			
3	+1			*Y*		
4	+1				*Y*	
5	+1					*Y*
6		−1		*Y*		
7		−1			*Y*	
8		−1				*Y*
9			+1	*Y*		
10			+1		*Y*	
11			+1			*Y*

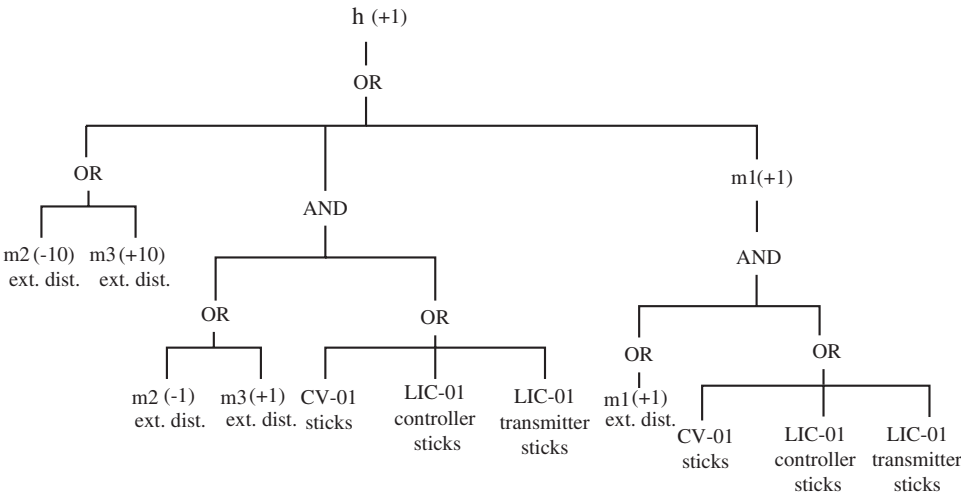

Fig. 4. Fault tree with top event "liquid level in tank T-01 is too high."

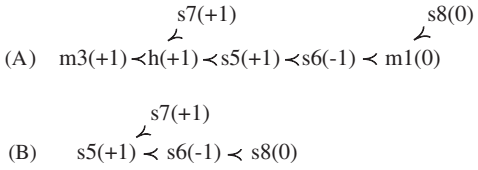

Fig. 5. (A) FPP of cut set 9 and (B) SOO of cut set 9.

Table 2
Candidate patterns of cut set 9 in Table 1

No.	$s5$	$s6$	$s7$	$s8$
1	0	0	0	0
2	+1	0	0	0
3	+1	0	+1	0
4	+1	−1	0	0
5	+1	−1	+1	0
6	+1	−1	0	0*
7	+1	−1	+1	0*

Table 3
IF–THEN inference rules of cut set 9 in Table 1

No.	IF				THEN
	$s5$	$s6$	$s7$	$s8$	cs_9
1	ZE	ZE	ZE	ZE	NOC
2	SP	ZE	ZE	ZE	UCT_1
3	SP	ZE	SP	ZE	UCT_2
4	SP	SN	ZE	ZE	UCT_2
5	SP	SN	SP	ZE	UCT_3
6	SP	SN	ZE	ZE	UCT_3
7	SP	SN	SP	ZE	OCR

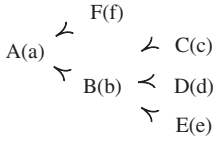

Fig. 6. A fictitious SOO.

complex than those studied previously. Such loops may be the result of applying advanced process control schemes, e.g., the cascade control systems, ratio control systems and override control systems, and/or due to coupled process dynamics. It should be noted that the inherent features in system dynamics caused by various different fault origins can be captured with several available diagnosis strategies, e.g., the trend identification (Bakshi and Stephanopoulos, 1994a,b; Dash et al., 2003) and PCA/wavelet analysis (Lu et al., 2003). However, since the data processing loads of these methods are quite heavy, there is still a need to develop a simpler approach.

Notice that prediction of the fault propagation behavior in a multi-loop process is in general very difficult since the net outcomes of various combinations of conflicting effects are usually indeterminable. However, it can also be observed that a controllable disturbance can always drive the loop variables in a *control* system, i.e., sensor signals, controller outputs, manipulated and controlled variables, to new steady states and these states can often be qualitatively determined, e.g., see Chang and Hwang (1992). Thus, the objective of the present research is to systematically enhance the capability of our previous fuzzy-logic-based fault diagnosis techniques for control systems with multiple loops. The more general problem of identifying fault origins in systems with coupled *process* dynamics is left for future study.

To illustrate the improvements achieved in the present work, the rest of this paper is organized as follows: in Section 2, the implementation procedure for a loop-free system is reviewed to facilitate later discussions. Simple algorithms are then presented in Section 3 for automatically generating the candidate patterns associated with any given tree-shaped SOO. A systematic SDG-based qualitative simulation procedure is then described in Section 4 to predict the propagation paths of any

Table 4
Candidate patterns of the fictitious SOO in Fig. 6

No.	*A*	*B*	*C*	*D*	*E*	*F*
1	0	0	0	0	0	0
2	a	0	0	0	0	0
3	a	b	0	0	0	0
4	a	b	0	0	e	0
5	a	b	0	d	0	0
6	a	b	0	d	e	0
7	a	b	c	0	0	0
8	a	b	c	0	e	0
9	a	b	c	d	0	0
10	a	b	c	d	e	0
11	a	0	0	0	0	f
12	a	b	0	0	0	f
13	a	b	0	0	e	f
14	a	b	0	d	0	f
15	a	b	0	d	e	f
16	a	b	c	0	0	f
17	a	b	c	0	e	f
18	a	b	c	d	0	f
19	a	b	c	d	e	f

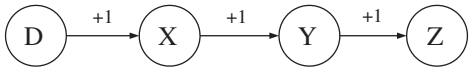

Fig. 7. A fictitious single-path SDG model.

Table 5
Candidate patterns derived from Eq. (8)

No.	*X*	*Y*	*Z*
1	0	0	0
2	+1	0	0
3	+10	0	0
4	+10	+1	0
5	+10	+10	0
6	+10	+10	+1
7	+10	+10	+10

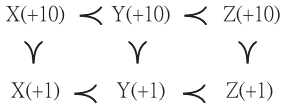

Fig. 8. The composite SOO of a single-path SDG.

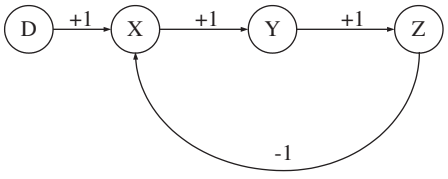

Fig. 9. A fictitious SDG model with a single feedback loop.

given fault origin in control systems with coupled feedback and/or feed forward loops. To further improve the diagnostic resolution of the fuzzy-logic-based strategy, a novel two-layer inference system has been devised accordingly to keep track of the historical trend of on-line measurements. The framework of this system is given in Section 5. Finally, the numerical simulation results of a series of extensive case studies are provided at the end of this paper to demonstrate the effectiveness of the proposed approach.

2. Implementation procedure for loop-free systems

To facilitate illustration of the improvements made in this work, a brief review of the implementation procedure of the fuzzy-logic-based fault diagnosis strategy for loop-free systems must be first presented. A more comprehensive version can be found either in Chang et al. (2002) or in Chang and Chang (2003). Let us use the level control system given in Fig. 2 as an example to illustrate the application steps outlined in Fig. 1. In this process, there are two input streams, i.e., streams 1 and 3, and one output stream, i.e., stream 2, connected to the liquid storage tank T-01. The level control loop consists of the level sensor, the proportional-integral (PI) controller LIC-01 and the control valve CV-01 on stream 1. The flow rates of streams 1 and 2 are also monitored with flow meters FI-01 and FI-02, respectively. It is assumed that the gate valve on the stream 2 (V-02) is open and the globe valve on stream 3 (V-03) closed during normal operation.

Table 6
Candidate patterns derived from Eq. (14)

No.	*X*	*Y*	*Z*
1	0	0	0
2	+1	0	0
3	+1	+1	0
4	+1	+1	+1
5	*x*	*y*	*z*

2.1. Signed directed graph, fault tree and minimal cut set

The SDG model of the level control system can be found in Fig. 3. The nodes in this digraph are mainly associated with the process variables, the measurement signals and the control signals. Specifically, the mass flow rates and instrument signals are represented, respectively, by combining an initial letter, i.e., *m* and *s*, with a numerical label. These numerical labels are basically the line numbers in the process flow diagram. Thus, $m1$ represents the mass flow rate of stream 1, and $s5$ is the measurement signal of liquid level in line 5. Finally, h denotes the actual height of liquid level.

In this work, a set of five values, i.e., $\{-10, -1, 0, +1, +10\}$, may be assigned to each node in a SDG to *qualitatively* represent deviation from the normal level of corresponding variable. The value 0 represents the normal steady state. The negative values are used to denote the lower-than-normal states and the positive values signify the opposite. The magnitudes of nonzero deviations, i.e., 1 or 10, can be interpreted qualitatively

$$\text{(A)}\quad s5(+1) \prec s6(-1) \prec s8(-1) \prec [s5(+1),\ s6(-10),\ s8(-10)]_f \quad (s7(+1);\ s7(+1)_f)$$

$$\text{(B)}\quad s5(+1) \prec s6(-1) \prec s8(-1) \prec s5(+10) \prec s6(-10) \prec s8(-10) \prec [s5(+1),\ s6(-10),\ s8(-10)]_f \quad (s7(+1);\ s7(+10);\ s7(+1)_f)$$

Fig. 10. Two possible SOOs of an uncontrollable disturbance from $m3$ in the level control system.

Table 7
Candidate patterns for SOO (A) in Fig. 10

No.	$s5$	$s6$	$s7$	$s8$
1	0	0	0	0
2	+1	0	0	0
3	+1	0	+1	0
4	+1	−1	0	0
5	+1	−1	+1	0
6	+1	−1	0	−1
7	+1	−1	+1	−1
8	+1	−10	+0	−10
9	+1	−10	+1	−10
10	+1	−10	+1	−10
11	+1	−10	+1	−10

as "small" and "large", respectively. Notice also that the causal relation between two variables under normal condition can be characterized with a directed arc and the corresponding gain. Each gain may also assume one of the above five qualitative values. The output value of an arc can be computed with the gain and its input value according to the following equation:

$$v_{\text{out}} = \begin{cases} g \times v_{\text{in}} & \text{if } -10 \leqslant g \times v_{\text{in}} \leqslant +10, \\ +10 & \text{if } g \times v_{\text{in}} > +10, \\ -10 & \text{if } g \times v_{\text{in}} < -10, \end{cases} \quad (1)$$

where g, v_{in} and v_{out} denote, respectively, the gain, input and output values. Finally, it should be noted that, other than the normal arc, one or more conditional arc may be added between two nodes. These arcs are valid only under the specified conditions.

Let us select the condition "high liquid level in the tank," i.e., $h(+1)$, as one of the top events for diagnosis purpose. The conventional Lapp-and-Powers algorithm (Chang and Hwang, 1992; Lapp and Powers, 1977) is adopted in this study to synthesize the fault tree in Fig. 4 on the basis of Fig. 3. The resulting minimal cut sets can be found in Table 1.

2.2. Symptom occurrence order

The effects of base event(s) identified in a cut set of the fault tree usually propagate throughout the entire system sequentially. In general, a series of intermediate events may occur before the inception of a designated undesirable consequence (top event). Since the performance of a diagnosis scheme should be evaluated not only in terms of its correctness but also its timeliness, it has been the intention of this research to develop a

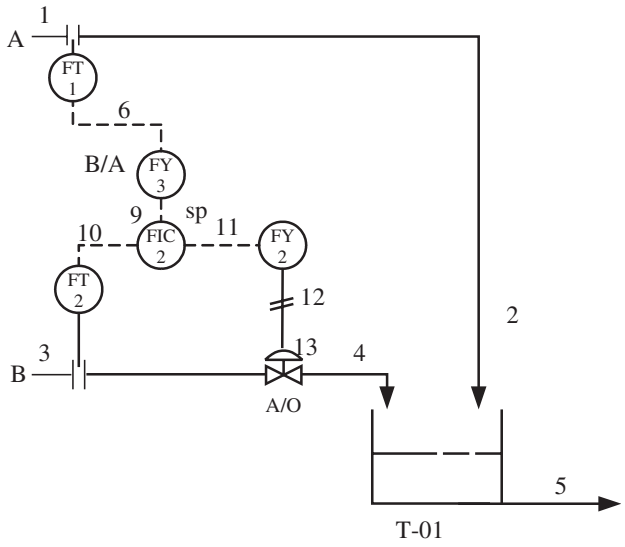

Fig. 11. A ratio control system.

fault identification procedure taking both the eventual symptoms and also their *occurrence order* into consideration.

To identify this SOO associated with a fault origin, the corresponding fault propagation behavior in the given system must be first established with a qualitative reasoning procedure. In fact, numerous studies have already been published on the subject of systematic *qualitative simulation* using the so-called qualitative differential equations (QDEs), e.g., see Kuipers (1994). Although the simulation results generated with QDEs are comprehensive, this approach is somewhat cumbersome in the present applications. In particular, these results cannot be directly encoded into the IF–THEN rules required in our FIS. Consequently, the SDG-based qualitative simulation techniques are developed instead in the present study. For illustration convenience, let us consider the basic events in the 9th cut set, i.e., $\{m3(+1)$, CV-01 sticks$\}$, as an example. It should be stressed that the configuration of digraph model in this case is changed under the influence of the failure "CV-01 sticks." Since the gain between nodes $s6$ and $m1$ now becomes zero, the resulting system should be considered as *loop free*. The effects of the above basic events can be simulated qualitatively according to two simple rules, i.e.,

- Given the input value, the output value of an arc in the SDG model can be computed on the basis of Eq. (1).
- The input is always affected earlier than output.

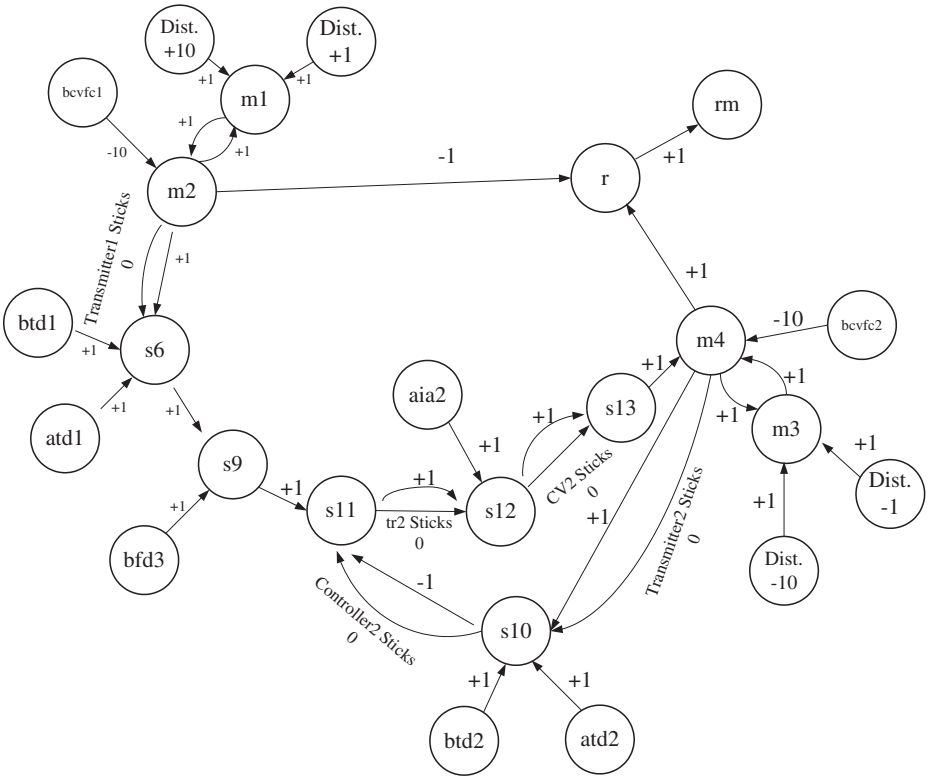

Fig. 12. Digraph model of the ratio control system in Fig. 11.

Table 8
Candidate patterns derived from Eqs. (16) and (17)

No.	$s6$	$s9$	$s10$	$s11$	$s12$	$s13$	$rm^{(1)}$	$rm^{(2)}$	rm
1	0	0	0	0	0	0	0	0	0
2	+1	0	0	0	0	0	0	0	0
3	+1	0	0	0	0	0	−1	0	−1
4	+1	+1	0	0	0	0	0	0	0
5	+1	+1	0	0	0	0	−1	0	−1
6	+1	+1	0	+1	0	0	0	0	0
7	+1	+1	0	+1	0	0	−1	0	−1
8	+1	+1	0	+1	+1	0	0	0	0
9	+1	+1	0	+1	+1	0	−1	0	−1
10	+1	+1	0	+1	+1	+1	0	0	0
11	+1	+1	0	+1	+1	+1	−1	0	−1
12	+1	+1	+1	+1	+1	+1	0	0	0
13	+1	+1	+1	+1	+1	+1	−1	0	−1
14	+1	+1	+1	+1	+1	+1	0	+1	+1
15	+1	+1	+1	+1	+1	+1	−1	+1	0

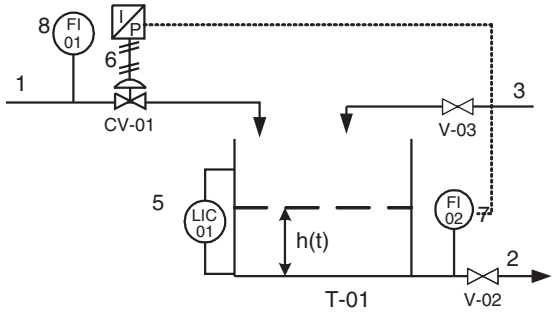

Fig. 13. A feed-forward level-control system.

Table 9
Candidate patterns for a large increase in the flow rate of stream A in the single-NFBL ratio-control system in Fig. 11

No.	$s6$	$s9$	$s10$	$s11$	$s12$	$s13$	$rm^{(1)}$	$rm^{(2)}$	rm
1	0	0	0	0	0	0	0	0	0
2	+10	0	0	0	0	0	0	0	0
3	+10	0	0	0	0	0	−10	0	−10
4	+10	+10	0	0	0	0	0	0	0
5	+10	+10	0	0	0	0	−10	0	−10
6	+10	+10	0	+10	0	0	0	0	0
7	+10	+10	0	+10	0	0	−10	0	−10
8	+10	+10	0	+10	+10	0	0	0	0
9	+10	+10	0	+10	+10	0	−10	0	−10
10	+10	+10	0	+10	+10	+10	0	0	0
11	+10	+10	0	+10	+10	+10	−10	0	−10
12	+10	+10	+10	+10	+10	+10	0	0	0
13	+10	+10	+10	+10	+10	+10	−10	0	−10
14	+10	+10	+10	+10	+10	+10	0	+10	+10
15	+10	+10	+10	+10	+10	+10	−10	+10	−1

The simulation results are depicted in Fig. 5(A), which will be referred to as the *fault propagation paths* (FPPs) in this paper. Notice that the structure of these paths is essentially the same as that of SDG and each node here represents a previously nonexistent fault effect. Every effect is specified with a qualitative value ± 1 or ± 10, which can be regarded as the degree of deviation from the normal state of an affected process variable. The precedence order of two different effects is specified by connecting them with the symbol $\prec$, i.e., the effect on its left should occur earlier than that on the right. The sequence of conditions on

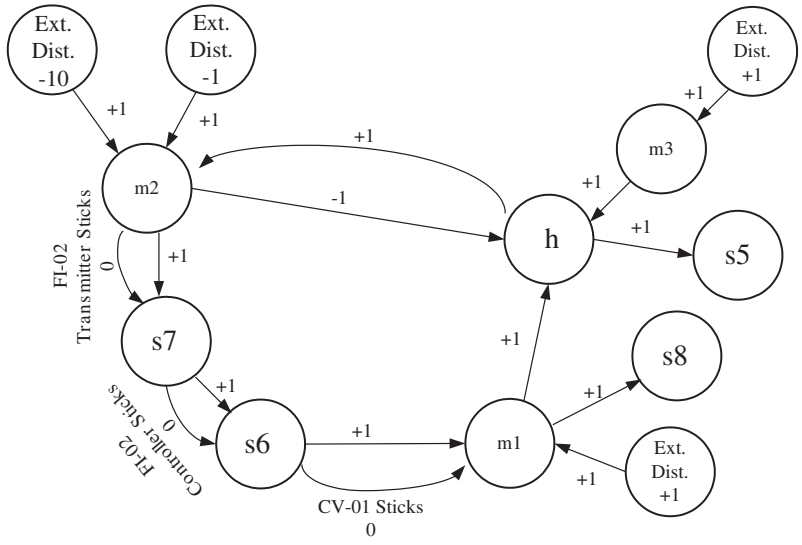

Fig. 14. Digraph model of feed-forward level-control system.

Table 10
Second-layer inference rules for the 4th pattern in Eq. (26)

No.	IF				THEN
	$p1^m$	$p2^m$	$p4^m$	$p6^m$	$sq3$
1	OCR	OCR	OCR	OCR	UCT_3
2	OCR	OCR	NOC	OCR	UCT_2
3	OCR	NOC	OCR	OCR	UCT_2
4	OCR	NOC	NOC	OCR	UCT_1

the same propagation path should be interpreted as the order of occurrence (in time) of various effects resulting from the given fault origin(s), while the order of two distinct events located on two separate branched paths should be considered as indeterminable. Finally, by merging every pair of measured variable and its measurement signal in the FPPs and then eliminating the unmeasured ones, the SOO shown in Fig. 5(B) can be obtained. This SOO represents the occurrence order of observable on-line symptoms.

2.3. Candidate patterns

If all symptoms in a SOO are detected on-line, then it is certainly reasonable to confirm the existence of corresponding fault origin(s). However, it is also possible to find that these symptoms are only partially developed during the incipient period of an eventual system hazard and, further, their pattern may vary at different times during operation. The collection of on-line symptoms at any time after the introduction of basic event(s) in a cut set is referred to as a *candidate pattern* in this work. It is obvious that any candidate pattern can be considered as an evidence for fault identification with a degree of confidence. Thus, it is important to enumerate all possible candidate patterns and evaluate their respective significance in the off-line preparation stage. In a loop-free system, the SOO always assumes the form of a tree. The total number of candidate patterns N_{CP} in this case can be computed with a formula derived by Chang et al. (2002):

$$N_{CP} = \mathcal{N}\{\mathbf{P}^{(0)}(n_0)\} = n_0 + \prod_{i_1=1}^{N_0} \mathcal{N}\{\mathbf{P}^{(0,i_1)}(n_{0,i_1})\}, \tag{2}$$

where $\mathbf{P}^{(0)}(n_0)$ denotes the initial path of length n_0 in the tree-shaped SOO; $\mathbf{P}^{(0,i_1)}(n_{0,i_1})$ $(i_1 = 1, 2, \ldots, N_0)$ denotes the i_1th branch path of length n_{0,i_1} connecting to the end of $\mathbf{P}^{(0)}(n_0)$; $\mathcal{N}\{\cdot\}$ denotes the counting operator of a given path. The results of counting operation can be obtained recursively, i.e.,

$$\begin{aligned}\mathcal{N}\{\mathbf{P}^{(0,i_1,i_2,\ldots,i_k)}(n_{0,i_1,i_2,\ldots,i_k})\} &= n_{0,i_1,i_2,\ldots,i_k} \\ &\quad + \prod_{i_{k+1}=1}^{N_{0,i_1,i_2,\ldots,i_k}} \mathcal{N}\{\mathbf{P}^{(0,i_1,i_2,\ldots,i_{k+1})}(n_{0,i_1,i_2,\ldots,i_k,i_{k+1}})\},\end{aligned} \tag{3}$$

where $k = 1, 2, \ldots$ and $\mathbf{P}^{(0,i_1,i_2,\ldots,i_k,i_{k+1})}(n_{0,i_1,i_2,\ldots,i_k,i_{k+1}})$ is the i_{k+1}th branch path connecting to the end of $\mathbf{P}^{(0,i_1,i_2,\ldots,i_k)}(n_{0,i_1,i_2,\ldots,i_k})$. If there are no further branches connected to the end of the branch path $\mathbf{P}^{(0,i_1,i_2,\ldots,i_k)}(n_{0,i_1,i_2,\ldots,i_k})$, i.e., $N_{0,i_1,i_2,\ldots,i_k} = 0$, then

$$\prod_{i_{k+1}=1}^{0} [\cdot] = 1. \tag{4}$$

By following this computation procedure, the number of candidate patterns associated with the SOO in Fig. 5(B) can be determined to be 7. The corresponding candidate patterns are listed in Table 2. Notice that there are two pairs of seemingly identical patterns. The first is associated with rows 4 and 6, and the second can be found in rows 5 and 7. This is mainly due to the fact that $s8(0)$ is treated as a symptom in SOO.

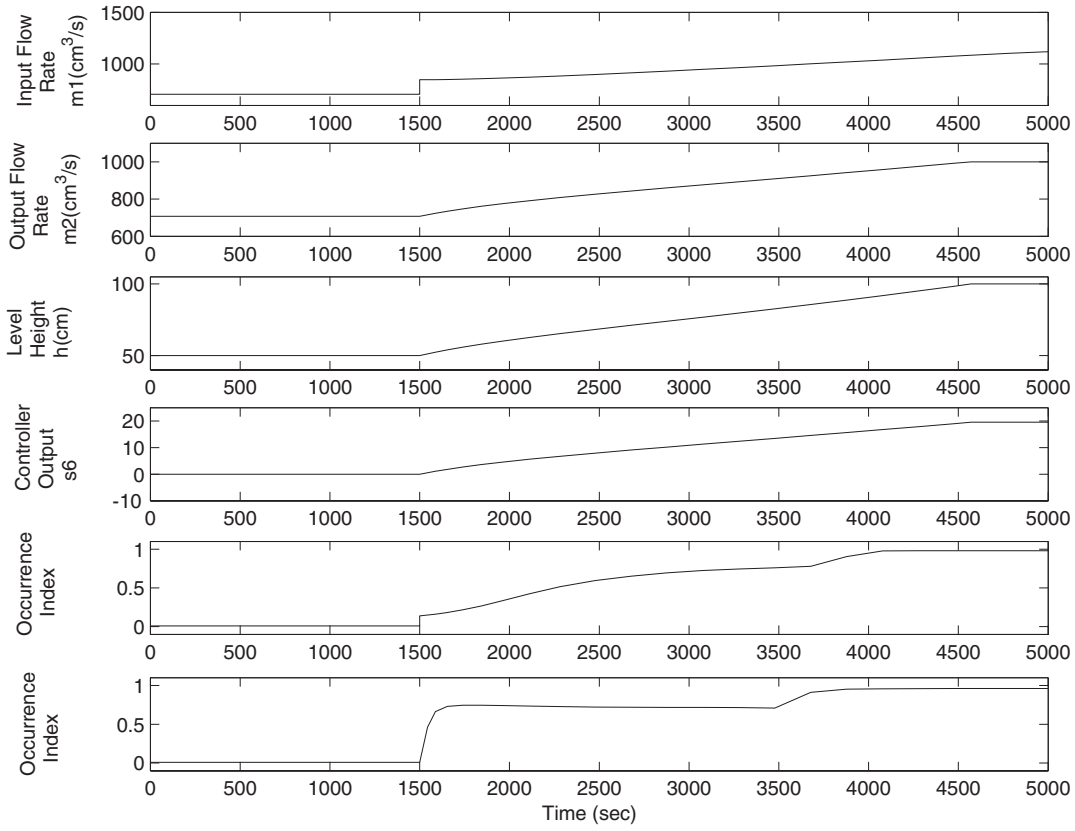

Fig. 15. Diagnosis results of conventional one-layer inference scheme using simulation data obtained by introducing a small increase in stream 1, i.e., $m1(+1)$, of the feed-forward level-control system in Fig. 13: (A) simulation data of input flow rate; (B) simulation data of output flow rate; (C) simulation data of level height; (D) simulation data of controller output; (E) occurrence index obtained with the assumed fault $m1(+1)$ and (F) occurrence index obtained with the assumed fault $m3(+1)$.

In other words, the patterns in each pair should be interpreted differently. In rows 6 and 7, asterisks are used to denote the fully developed symptoms. On the other hand, the corresponding unmarked 0 in row 4 or 5 indicates that the effects of abnormal disturbances have not reached the flow sensor FI-01.

2.4. IF–THEN rules

Each candidate pattern can be encoded into an IF–THEN rule to evaluate the existence potential (or occurrence index) of the corresponding cut set with a fuzzy inference engine. For example, the patterns in Table 2 can be converted one-by-one into the inference rules listed in Table 3 according to the following *linguistic interpretation function F*:

$$F(\delta_j) = \begin{cases} \text{LN} & \text{if } \delta_j = -10, \\ \text{SN} & \text{if } \delta_j = -1, \\ \text{ZE} & \text{if } \delta_j = 0, \\ \text{SP} & \text{if } \delta_j = +1, \\ \text{LP} & \text{if } \delta_j = +10, \end{cases} \tag{5}$$

where δ_j denotes the qualitative deviation value of the jth measurement; LN, SN, ZE, SP and LP denote, respectively, the linguistic values of -10, -1, 0, $+1$ and $+10$.

If the on-line symptoms are identical to those in a SOO, then it is highly possible that they are caused by the corresponding fault origin. Consequently, the last rule in Table 3 can be used to assert such a belief. Here, OCR is a linguistic value of the occurrence index of cut set 9, i.e., cs_9. This value is used to reflect the highest confidence in confirming the existence of corresponding fault origin(s). On the other hand, it is quite reasonable to disregard the possibility of a fault if none of the symptoms in the corresponding SOO can be observed. Thus, the first rule in the same table should also be incorporated in the FIS. In this rule, NOC is the linguistic value reflecting the lowest confidence. The remaining candidate patterns are translated into rules with uncertain conclusions (subsequents), i.e., UCT_ℓ. The antecedents of each rule can be determined by substituting the qualitative deviation values in a candidate pattern into the linguistic interpretation function F. The number of matched transient and final symptoms in the candidate pattern is used as the degree of confidence ℓ in conclusion UCT_ℓ.

2.5. On-line implementation

In practical applications, the on-line measurement data should be first compared with the normal steady-state values of the process variables. The process deviations can be determined in real time and then used as the inputs to a FIS for computing the occurrence indices of fault origins. The

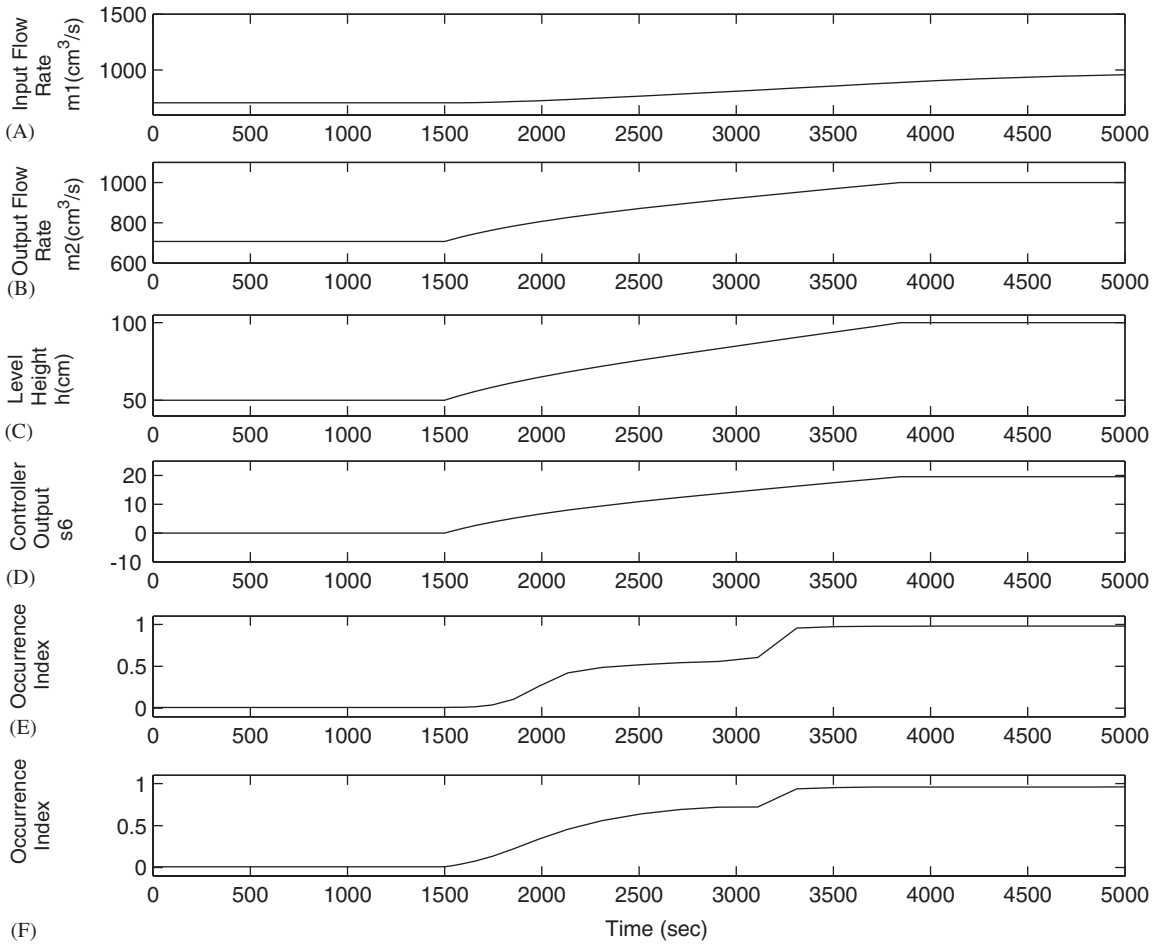

Fig. 16. Diagnosis results of conventional one-layer inference scheme using simulation data obtained by introducing a small increase in stream 3, i.e., $m3(+1)$, of the feed-forward level-control system in Fig. 13: (A) simulation data of input flow rate; (B) simulation data of output flow rate; (C) simulation data of level height; (D) simulation data of controller output; (E) occurrence index obtained with the assumed fault $m1(+1)$ and (F) occurrence index obtained with the assumed fault $m3(+1)$.

membership functions used in this study for classifying the process deviations and occurrence indices are the same as those adopted in Chang and Chang (2003). For the sake of brevity, detailed descriptions of these functions are not included in this paper.

3. Pattern generation algorithms

It should be noted that Eqs. (2)–(4) can only be used to compute the total number of candidate patterns. The actual patterns themselves were created *manually* according to the definition of SOO in the previous studies (Chang and Chang, 2003; Chang et al., 2002). This task inevitably becomes laborious and error-prone as the size of SOO grows. Thus, there is a need to develop systematic algorithms to automatically generate all candidate patterns associated with any given tree-shaped SOO.

To fix idea, let us consider the fictitious SOO presented in Fig. 6. In each node of this SOO, the capital letter is used to represent a process variable and the lower-case letter in parenthesis denotes its qualitative deviation value. An exhaustive search of this structure can be performed efficiently with a procedure given in Horowitz and Sahni (1984). Every node in the tree is guaranteed to be visited exactly once in the search process. Since the structural property of SOO is kept in the search record, it is used in this work as the basis for pattern generation. For example, a possible record resulting from a search on the SOO in Fig. 6 may be: $A(a)B(b)E(e)D(d)C(c)F(f)$. Notice that, although there are other possibilities, it can be shown that the choice of search record does not really affect the candidate patterns produced with the enumeration approach described below.

The candidate patterns can be generated by processing the items in the search record one-by-one. Obviously, the initial pattern associated with the first item should be $\{A(a), B(0), C(0), D(0), E(0), F(0)\}$. This pattern can be written in an abbreviated form $\{A\}$ by removing all symptoms with zero deviations and also dropping the nonzero deviation value of the occurred symptom. By definition, the occurrence order of the symptoms must follow SOO. Thus, the symptom $A(a)$ must have already occurred by the time when the symptom $B(b)$ occurs. In other words, the candidate pattern corresponding to the second item in the search record can

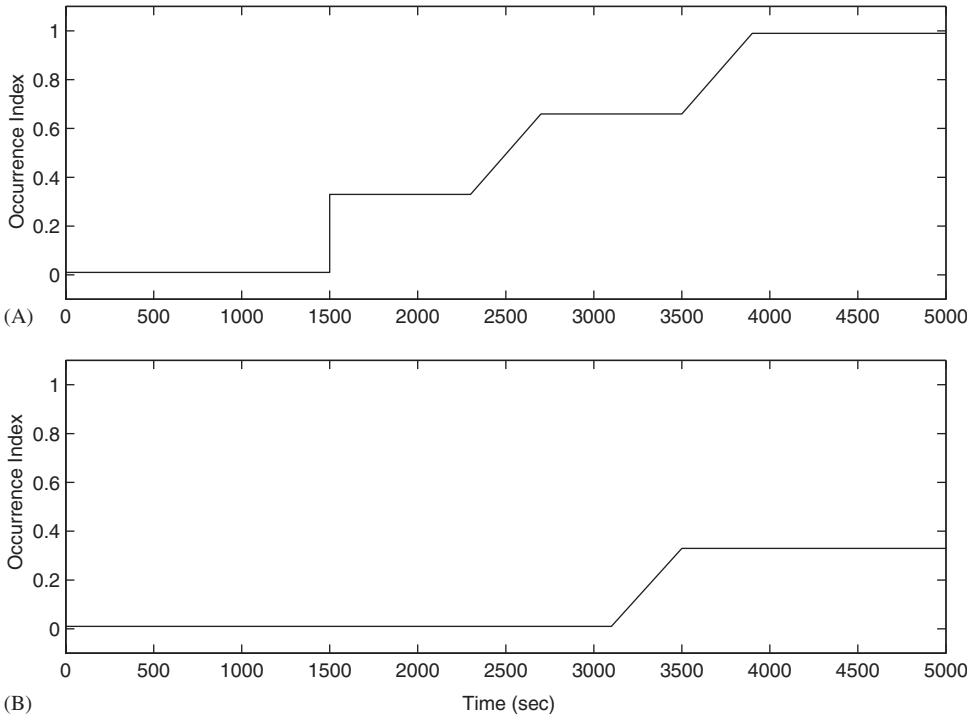

Fig. 17. Diagnosis results of the proposed two-layer inference scheme using simulation data obtained by introducing a small increase in stream 1, i.e., $m1(+1)$, of the feed-forward level-control system in Fig. 13. (A) occurrence index obtained with the assumed fault $m1(+1)$ and (B) occurrence index obtained with the assumed fault $m3(+1)$.

be obtained by inserting an additional symptom $B(b)$ into a previously constructed pattern which contains its immediate predecessor in SOO, i.e., $A(a)$. More specifically, this operation yields the pattern $\{A, B\}$. The candidate patterns associated with the third item $E(e)$ in search record can also be produced by inserting the corresponding symptom into the available pattern(s) containing its predecessor $B(b)$. Since the completed patterns at this point is $\{A\}$ and $\{A, B\}$, the latter can be adopted to generate a new pattern $\{A, B, E\}$. The 4th item $D(d)$ in search record can be processed in a similar fashion. From Fig. 6, it can be observed that the predecessor of the node corresponding to this item is also $B(b)$. Thus, the new patterns in this case should be $\{A, B, D\}$ and $\{A, B, D, E\}$. The candidate patterns associated with the remaining items in search record have been created with exactly the same approach. As a result, a total of 18 candidate patterns can be derived from the SOO in Fig. 6 and they are all presented in Table 4.

This proposed approach can be summarized in the following algorithms:

(1) *Construction of search record*
   (a) Starting from the root node of the tree-shaped SOO, visit and record every node on the initial path in sequence until reaching a branch node.
   (b) Arbitrarily select a branch path.
   (c) Visit and record every node on the selected path in sequence until reaching another branch node.
   (d) Repeat steps (b) and (c) until reaching an end node.
   (e) Return to the nearest branch node upstream with one or more branch path which has not been visited before. Apply steps (b)–(d) to this branch node. If no unprocessed paths can be found, the search should be terminated.

(2) *Generation of candidate patterns*
   (a) Let $k = 1$. Produce a single-symptom candidate pattern associated with the first item of search record.
   (b) let $k = k + 1$.
   (c) Produce the candidate patterns associated with the kth item in search record.
      (i) Locate the node in SOO which is identical to the kth item of search record. From the previously constructed patterns, select the ones that contain the predecessor of this node in SOO.
      (ii) Insert the kth item in search record into the selected patterns to create additional new patterns.
   (d) Repeat steps (b) and (c) until k equals the record length.

The above algorithms have been coded with C++ and tested extensively with different SOOs.

Finally, it should also be noted that the task of translating the candidate patterns into IF–THEN rules is relatively straightforward. By applying the linguistic interpretation function defined in Eq. (5) and setting the degree of confidence ℓ in the linguistic value UCT_ℓ to be the number of occurred symptoms, the candidate patterns in Table 4 can be easily converted to the inference rules. This translation procedure has also been incorporated in the same computer program mentioned above.

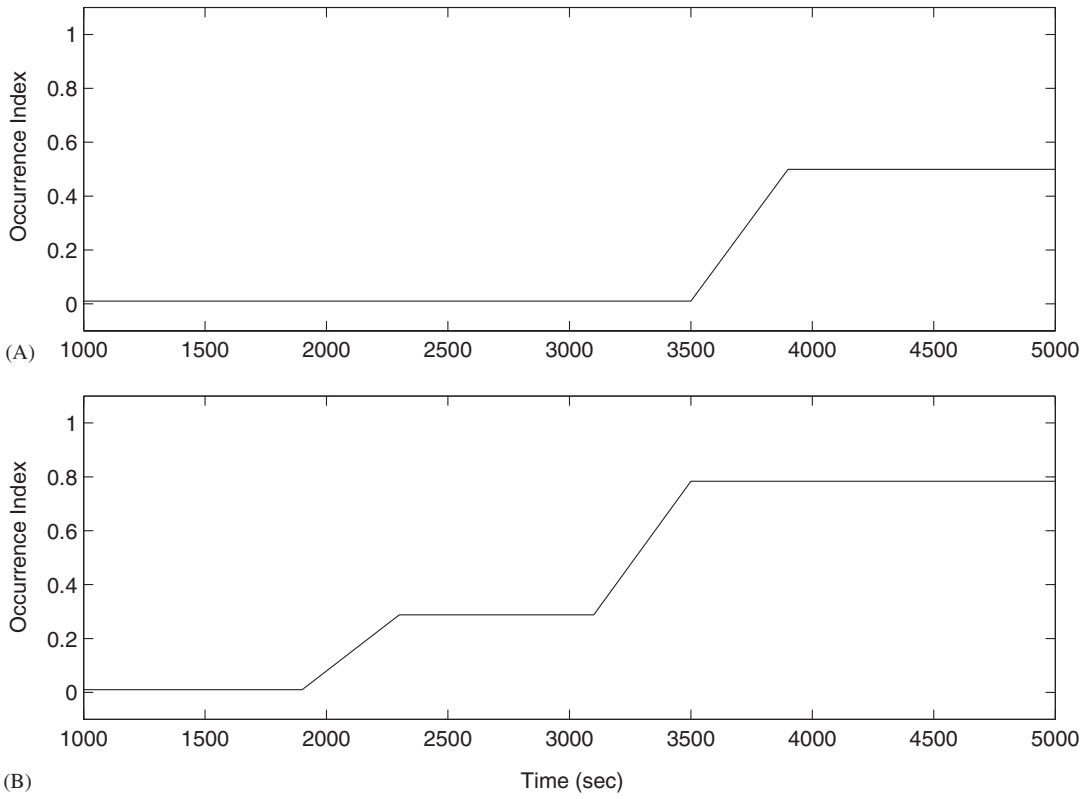

Fig. 18. Diagnosis results of the proposed two-layer inference scheme using simulation data obtained by introducing a small increase in stream 3, i.e., $m3(+1)$, of the feed-forward level-control system in Fig. 13. (A) occurrence index obtained with the assumed fault $m1(+1)$ and (B) occurrence index obtained with the assumed fault $m3(+1)$.

4. Candidate patterns in control systems with coupled loops

In a loop-free system, the net effect of fault propagation on a process variable can be viewed qualitatively as the direct transition from its normal state to another new state. However, if a process contains feedback and/or feed forward loops, the intermediate transient states must also be considered. Although a systematic procedure has already been developed in Chang and Chang (2003) to generate the candidate patterns in a feedback control system, there are still needs for further studies since this previous method is applicable only to the single-loop processes with specific limiting constraints imposed upon the "speed" of control action. A more comprehensive analysis has been performed in this work and the resulting pattern-generation strategies are presented in the sequel:

4.1. Single feedback loop

Let us again consider the level control system presented in Fig. 2. It can be observed from Table 1 that the fault origins can be classified into two groups. The fault propagation behaviors caused by the basic events specified in the last nine cut sets, i.e., from the 3rd set to the 11th set, have already been analyzed in the previous sections. In each case, the feedback loop embedded in digraph model is broken due to an equipment failure and thus the system can be considered as *loop free*. On the other hand, the fault origins given in the first two cut sets do not affect the digraph configuration at all. They should be regarded as the uncontrollable disturbances that saturate the control loop.

4.1.1. Fault propagation mechanisms of large disturbances along a single path

To predict the candidate patterns created by any uncontrollable disturbance to a feedback control loop, it is necessary to first understand its fault propagation mechanism along a single path. For illustration convenience, let us consider the fictitious SDG presented in Fig. 7 and assume that all process variables, i.e., X, Y and Z, are measured. The SOO associated with a moderate-size disturbance $D(+1)$ can be written as

$$X(+1) \prec Y(+1) \prec Z(+1). \tag{6}$$

Notice that the construction rules of this SOO have already been outlined in Section 2.2.

The SOO associated with a large disturbance $D(+10)$ can be determined with the same rules if fault propagation is immediate and the transient states of the process variables can be neglected. Specifically, the SOO in this case can be expressed as

$$X(+10) \prec Y(+10) \prec Z(+10). \tag{7}$$

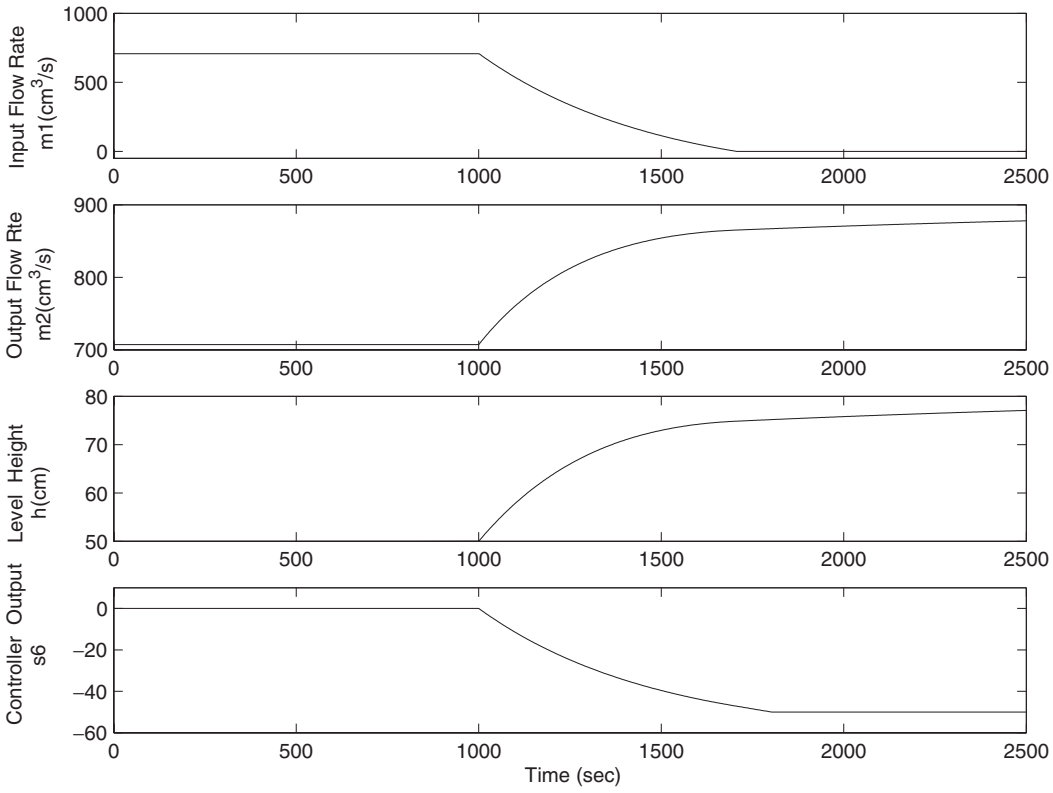

Fig. 19. Dynamic response caused by an uncontrollable disturbance in $m3$ of the level control system in Fig. 2.

However, if a finite time constant is needed to characterize the disturbance propagation behavior between two adjacent variables (say, from D to X), an additional rule must be introduced to facilitate a more accurate description of the effects caused by $D(+10)$, i.e., *the smaller deviation of a process variable must occur before reaching a larger one of the same variable*. Thus, a possible SOO of the "large" disturbance can be written accordingly

$$X(+1) \prec X(+10) \prec Y(+1) \prec Y(+10) \prec Z(+1) \prec Z(+10). \quad (8)$$

Notice that every process variable in this SOO assumes two distinct qualitative values. According to the definition of SOO, the earlier symptom of a process variable should be overridden by a later one observed in the same variable. On the basis of this *override rule*, all candidate patterns in Table 5 can be easily produced by inspection.

It should be noted that the disturbance $D(+10)$ may result in more than one SOO under the same condition. For example, if the propagation time for the effect of a moderate disturbance in Y to reach Z is shorter than the time needed for this disturbance to grow to the magnitude 10, the corresponding SOO should be modified as

$$X(+1) \prec X(+10) \prec Y(+1) \prec Z(+1) \prec Y(+10) \prec Z(+10). \quad (9)$$

If the relative propagation speeds of these two different effects are unknown, then Eqs. (8) and (9) should both be used for generating the candidate patterns. For the sake of completeness, three other possibilities are also listed below without further elaborations:

$$X(+1) \prec Y(+1) \prec X(+10) \prec Y(+10) \prec Z(+1) \prec Z(+10), \quad (10)$$

$$X(+1) \prec Y(+1) \prec X(+10) \prec Z(+1) \prec Y(+10) \prec Z(+10), \quad (11)$$

$$X(+1) \prec Y(+1) \prec Z(+1) \prec X(+10) \prec Y(+10) \prec Z(+10). \quad (12)$$

If a priori knowledge of the fault propagation dynamics is unavailable, the SOOs given in Eqs. (8)–(12) should all be included to generate the candidate patterns. However, it is also obvious that some of the resulting patterns are redundant, e.g., the first 3 patterns generated from Eq. (10) should be identical to those from Eq. (11). It is therefore necessary to integrate these SOOs with a composite SOO (see Fig. 8) to facilitate efficient enumeration of all possible candidate patterns.

Let us consider a generalized composite SOO with 2 rows and n columns. If the first k large-deviation (± 10) symptoms are present in a candidate pattern, then the first k moderate-deviation (± 1) symptoms must have already occurred. Since the remaining moderate-deviation symptoms may or may not be observable, the number of possible patterns with exactly k

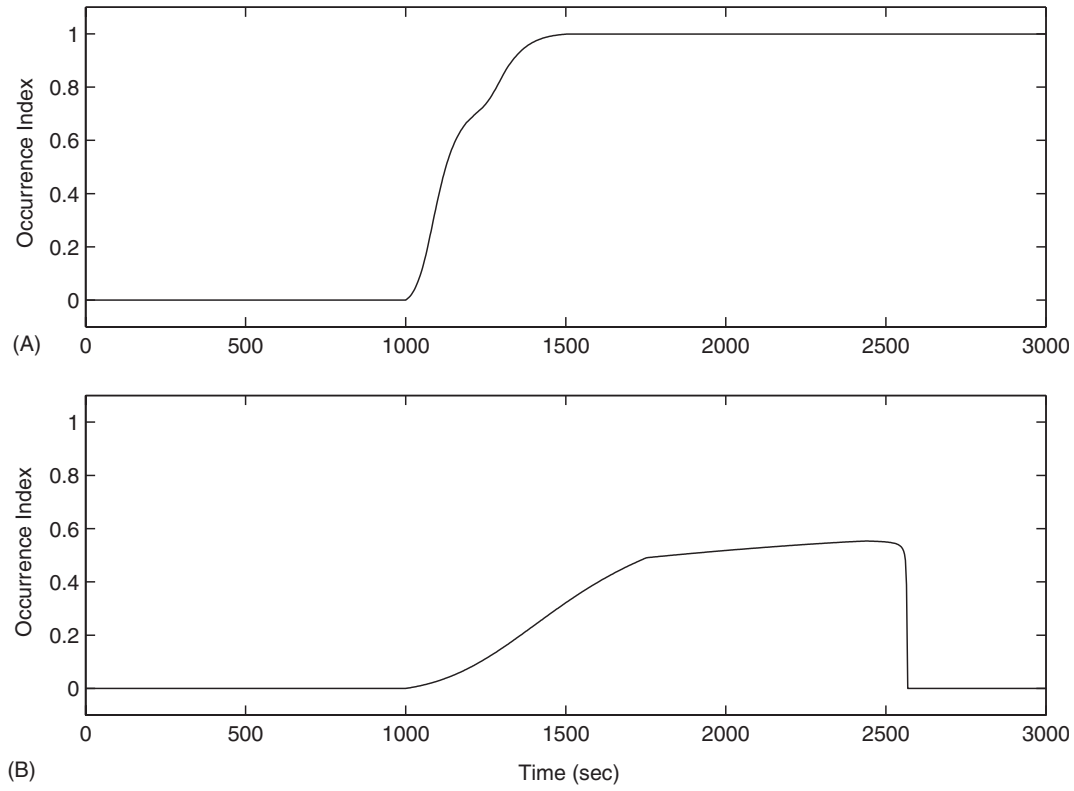

Fig. 20. Diagnosis results of two different scenarios in the level control system described in Fig. 2: (A) occurrence index of cut set 2 using simulation data obtained by introducing the basic event in cut set 2, i.e., an uncontrollable increase in stream 3 [$m3(+10)$] and (B) occurrence index of cut set 2 using simulation data obtained by introducing the basic events in cut set 9, i.e., a controllable increase in stream 3 [$m3(+1)$] and CV-01 sticks.

large-deviation symptoms should be $n-k+1$, and the total number of all candidate patterns should be

$$N_{CP}=\sum_{k=0}^{n}(n-k+1)=\frac{(n+1)(n+2)}{2}. \tag{13}$$

The pattern generation algorithms described previously in Section 3 are also applicable here after minor modifications. In particular, the selection criteria adopted in steps 1(b) and 2(c) should be changed as follows:

- *Step* 1(b): The predecessors of the starting node in the selected branch path in SOO should *all* be present in the search record.
- *Step* 2(c): Locate the node in SOO which is identical to the *k*th item of search record. The predecessors of this node should *all* be present in the selected candidate patterns.

4.1.2. Fault propagation mechanisms of uncontrollable disturbances in a negative feedback loop

Next, let us consider the fault propagation behaviors in the fictitious feedback loop shown in Fig. 9. The initial effects of a disturbance in D can be represented by one of the SOOs specified in Eqs. (8)–(12). However, it should also be noted that these SOOs may not be fully developed to the last symptom $Z(+10)$ in practice, since the implied compensation action of the negative feedback mechanism could come into effect right after the occurrence of intermediate state $Z(+1)$. For example, let us consider an initial propagation path described by Eq. (12). In this case, it can be assumed that the disturbance propagation processes from X to Y and Y to Z are almost immediate. If the same can be assumed concerning the propagation behavior between Z and X, then the corresponding SOO can be written as

$$X(+1)\prec Y(+1)\prec Z(+1)\prec\cdots\prec[X(x),Y(y),Z(z)]_f. \tag{14}$$

Otherwise, the SOO is

$$X(+1)\prec Y(+1)\prec Z(+1)\prec X(+10)\prec Y(+10)\prec Z(+10)\prec\cdots\prec[X(x),Y(y),Z(z)]_f. \tag{15}$$

Notice that, without quantitative knowledge about the physical parameters of the control system, the transient variations between the incipient and eventual states cannot be described explicitly in the above SOOs. These transient states can only be determined on a case-by-case basis if additional information is available in actual applications. Notice also that, in every SOO, the final states of loop variables are lumped into a single node in a square bracket and their precedence order is left unspecified. This is due to the difficulties in verifying the occurrence order of these symptoms in real time. Finally, x, y and z represent, respectively, the final steady-state values of X, Y and Z, and they should be determined with the qualitative simulation method proposed by Ju et al. (2004).

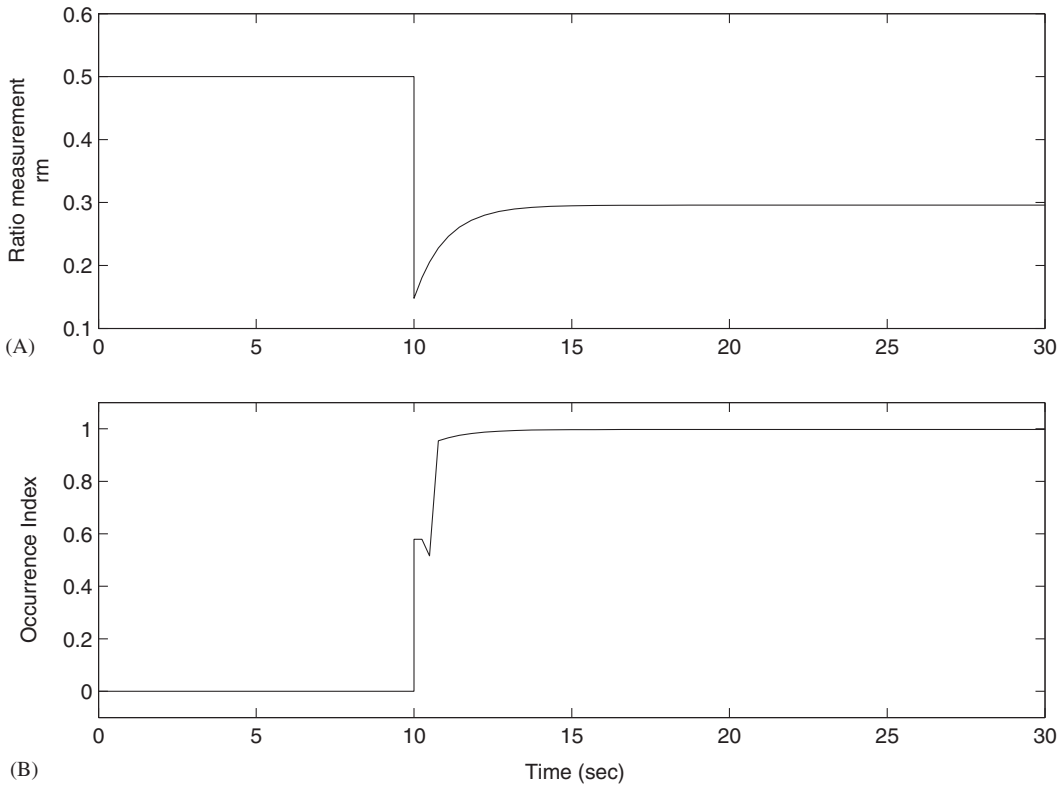

Fig. 21. Diagnosis results using simulation data obtained by introducing a large increase in the flow rate of stream A in the single-NFBL ratio-control system in Fig. 11: (A) dynamic response of flow-ratio measurement and (B) occurrence index of the correct fault origin.

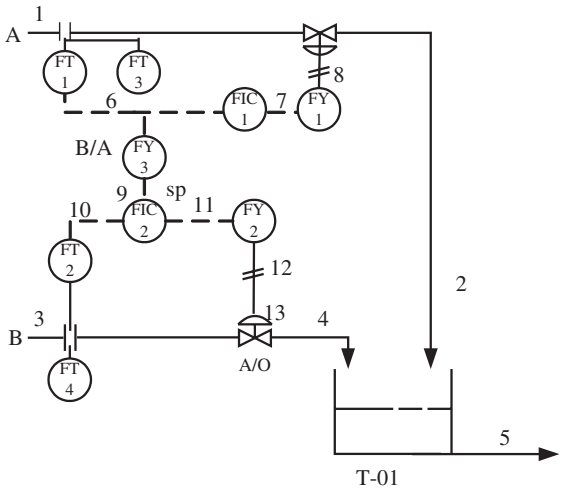

Fig. 22. A continuous stirred-tank reactor with a double-NFBL ratio-control system.

As long as the suitable SOO for a particular application is available, the candidate patterns can be generated according to the standard procedure described previously. For example, the candidate patterns in Table 6 can be produced from the SOO in Eq. (14). Let us next return to the level control example given in Fig. 2. From the fact that the transfer function between the flow rate of stream 3 and the height of liquid level is basically of first order, it is clear that the effects of an uncontrollable disturbance in $m3$ can be characterized qualitatively on the basis of the SOOs given in Eqs. (14) and/or (15). More specifically, the two possible occurrence orders in this case are shown in Fig. 10 and the candidate patterns derived from SOO (A) in this figure can be found in Table 7.

4.2. Single feed forward loop

A simple example is used here to illustrate the pattern generation procedure for systems with a single feed forward loop. Specifically, let us consider the production of caprolactam with cyclohexance oxime (reactant A) and oleum (reactant B) in a continuous reactor. The feed ratio of B to A is required to be maintained at a desired value for avoiding the hazardous condition of high reaction temperature due to rapid polymerization of cyclohexanone oxime. The piping and instrumentation (P&ID) of this process is presented in Fig. 11. In this system, the flow measurement signal of reactant A is used to adjust the set point of flow controller of reactant B. The corresponding SDG model is presented in Fig. 12. Notice that a two-path feed forward loop is embedded in this model, i.e., (1) $m2 \rightarrow r$ and (2) $m2 \rightarrow s6 \rightarrow s9 \rightarrow s11 \rightarrow s12 \rightarrow s13 \rightarrow m4 \rightarrow r$, and the second path is partially overlapped with a feedback loop, i.e., $s11 \rightarrow s12 \rightarrow s13 \rightarrow m4 \rightarrow s10 \rightarrow s11$. Although the above two loops are tangled, the fault propagation behavior

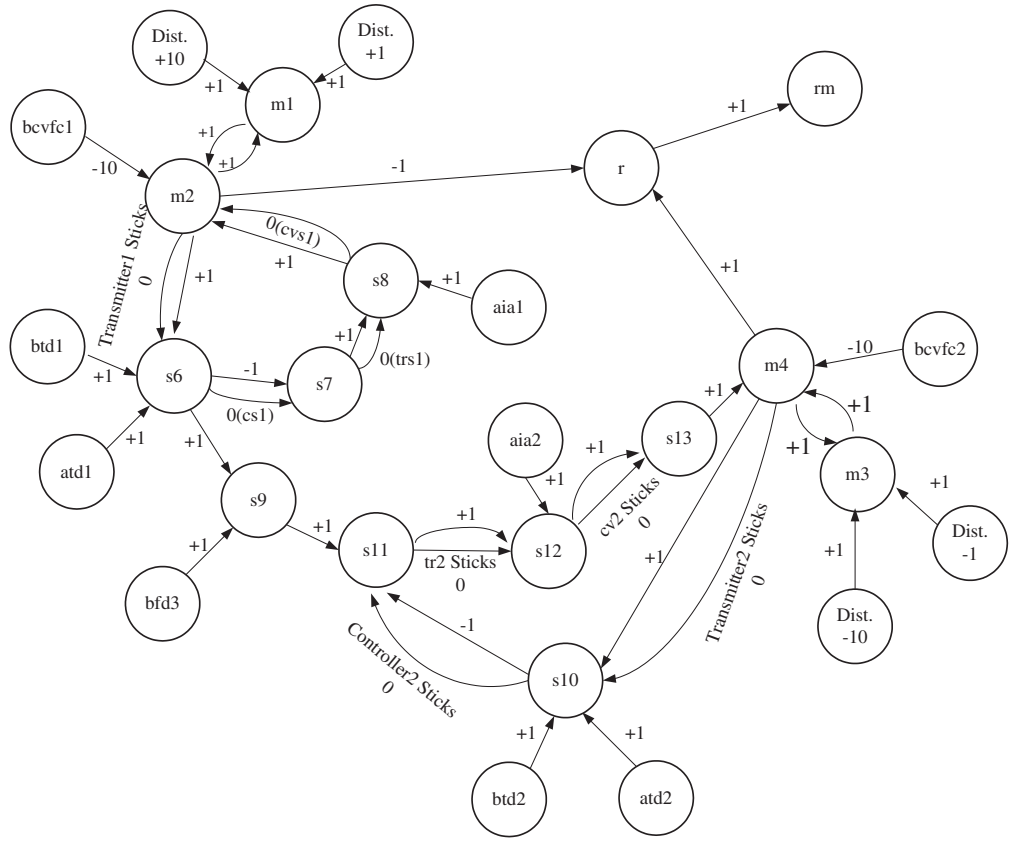

Fig. 23. Digraph model of the CSTR with double-NFBL ratio-control system.

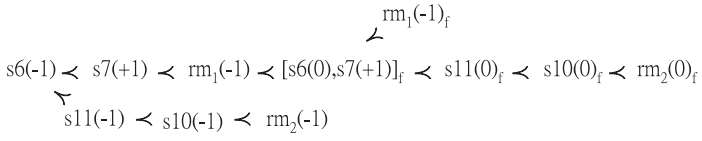

Fig. 24. SOO resulting from a bias failure in the flow sensor of stream A in the double-NFBL ratio-control system.

along the second path of the feed forward loop is actually *not* affected by the feedback mechanism since node $s9$ is the set point of flow controller.

Let us first consider the effects of a moderate increase in the flow rate of reactant A. The corresponding tree-shaped SOO consists of the following two branches:

$$s6(+1) \prec \mathrm{rm}^{(1)}(-1) \tag{16}$$

$$s6(+1) \prec s9(+1) \prec s11(+1) \prec s12(+1) \prec s13(+1) \prec s10(+1) \prec \mathrm{rm}^{(2)}(+1). \tag{17}$$

Notice that in this case the flow ratio r is assumed to be observable since the flows of reactants A and B are both measured on-line. The symbols $\mathrm{rm}^{(1)}$ and $\mathrm{rm}^{(2)}$ are used in this SOO to denote the changes in flow-ratio measurement caused by disturbances propagated along paths (1) and (2), respectively. The candidate patterns can then be produced by directly applying the proposed pattern generation algorithms to Eqs. (16) and (17). The resulting patterns can be found in Table 8. It should be noted that $\mathrm{rm}^{(1)}(-1)$ and $\mathrm{rm}^{(2)}(+1)$ are essentially two separate effects of an upstream disturbance on the same variable. Thus, the net change in flow ratio must also be evaluated since only rm is the observable variable. In this study, the variations in flow-ratio measurement are estimated by adding the qualitative values of $\mathrm{rm}^{(1)}$ and $\mathrm{rm}^{(2)}$ (see the last column of Table 8). This is due to the fact that, by definition, the opposite effects travelling along two separate paths in a feed forward control system must cancel out eventually.

If the above control loop could be saturated by uncontrollable disturbances, then the effects of a large increase in the flow of reactant A, i.e., $m1(+10)$, should be analyzed. To simplify our presentation, let us assume that the effects of this disturbance are propagated almost instantaneously and the transient states of all process variables can be neglected completely. In other words, the SOO in this case can be constructed simply by replacing ± 1 in Eqs. (16) and (17) by ± 10. Again, the corresponding candidate patterns in Table 9 can be easily obtained with the pattern generation algorithms described previously.

4.3. Coupled feed forward and/or feedback loops

The procedure to generate candidate patterns in systems with coupled loops is in principle *the same* as that described previously. The critical step is to produce a SOO with the proposed

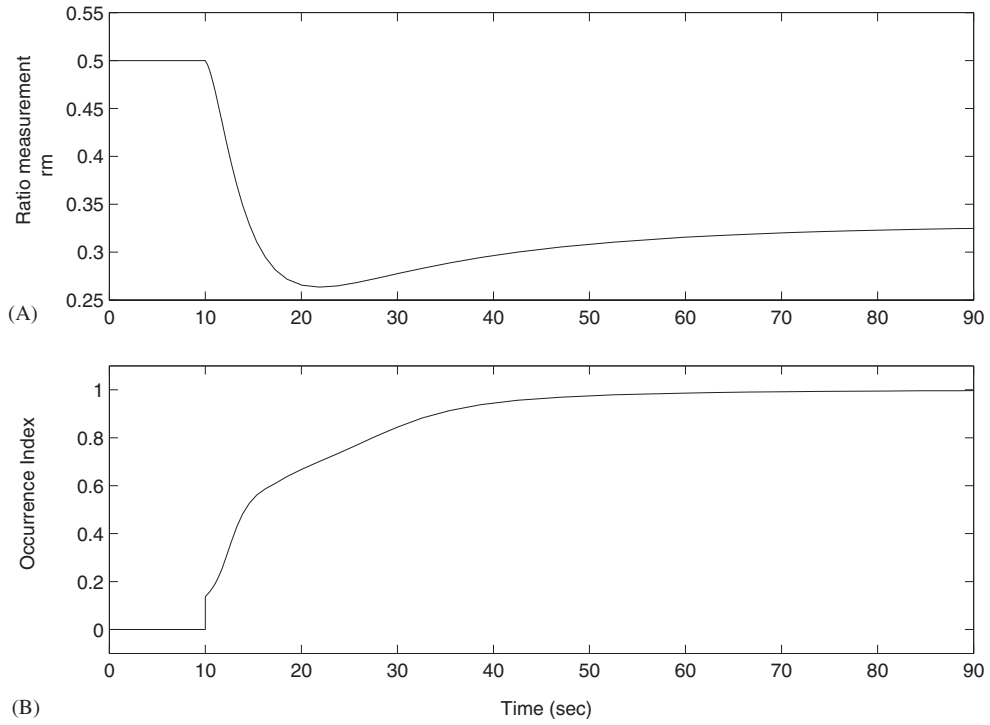

Fig. 25. Diagnosis results using simulation data obtained by introducing a bias failure in the flow sensor of stream A in the double-NFBL ratio-control system given in Fig. 22: (A) dynamic response of flow-ratio measurement and (B) occurrence index of the correct fault origin.

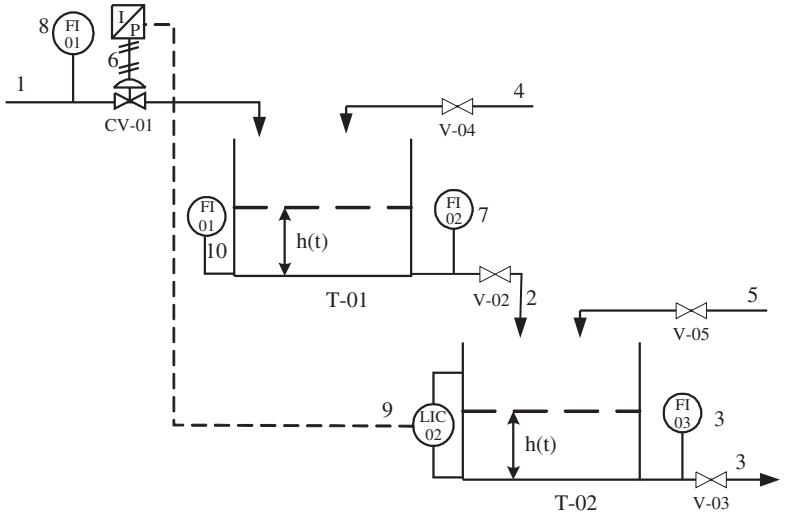

Fig. 26. A level control system with two tanks in series.

construction rules. Since this SOO is inevitably very complex, it is desirable to further simplify its structure on the basis of available process knowledge about the disturbance propagation dynamics. Let us consider the level control system presented in Fig. 13. Notice that a feed-forward control scheme is adopted here, i.e., the flow rate of stream 1 is manipulated according the measurement signal of stream 2 to keep the liquid level at a given height. Although this control strategy is unrealistic in the sense that only the downstream disturbances can be compensated by varying the input flow, the present example is still used mainly for illustration convenience. In particular, from the corresponding digraph model given in Fig. 14, it can be observed that this system contains two interacting loops. One of them is the feed forward loop caused by the control mechanism, i.e., $m2 \rightarrow h$ and $m2 \rightarrow s7 \rightarrow s6 \rightarrow m1 \rightarrow h$, and the other is the negative feedback loop formed naturally in the physical process, i.e., $m2 \rightarrow h \rightarrow m2$. Notice also that, since the end node of the former loop is a node on the latter, they can be viewed alternatively as two feedback loops sharing a common path $h \rightarrow m2$.

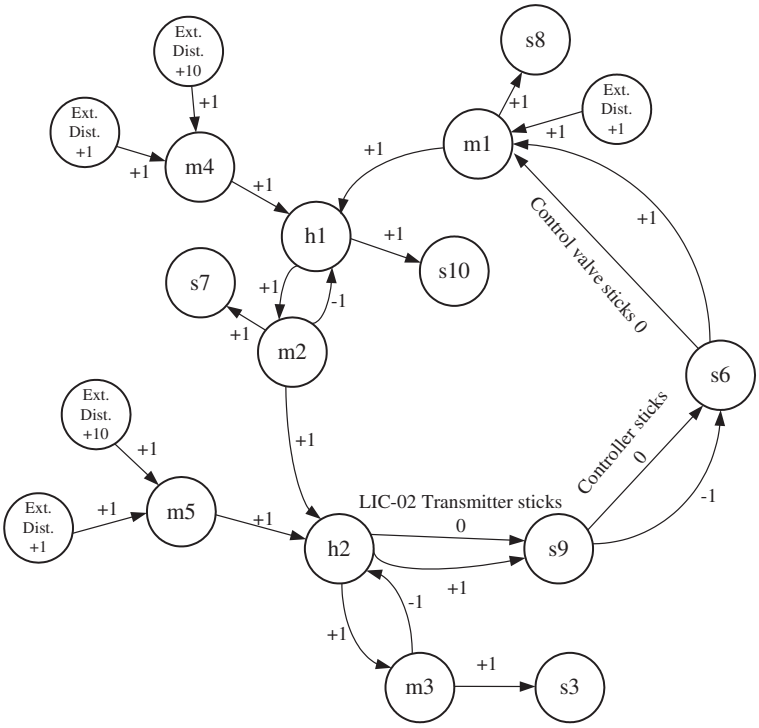

Fig. 27. Digraph model of the level control system in Fig. 26.

$$\text{(A)}\quad s10(+1) \prec s9(+1) \prec s(-1) \prec s8(-1) \prec s10(+10) \prec s9(+10) \prec s6(-10) \prec s8(-10) \prec [s10(+1),s9(+1),s6(-10),s8(-10)]_f \prec s3(+1)_f$$

$$\text{(B)}\quad s10(+1) \prec s10(+10) \prec s9(+1) \prec s6(-1) \prec s8(-1) \prec [s10(+1),s9(+1),s6(-10),s8(-10)]_f \prec s3(+1)_f$$

$$\text{(C)}\quad s10(+1) \prec s9(+1) \prec s6(-1) \prec s8(-1) \prec [s9(+1),s6(-10),s8(-10),s10(+1)]_f \prec s3(+1)_f$$

Fig. 28. All possible SOOs caused by a large positive disturbance in the flow rate of stream 4 in the two-tank system.

$$\text{(A)}\quad s9(+1) \prec s6(-1) \prec s8(-1) \prec s9(+10) \prec s6(-10) \prec s8(-10) \prec s10(-1) \prec s10(-10) \prec [s9(+1),s6(-10),s8(-10),s10(-10)]_f \prec s3(+1)_f$$

$$\text{(B)}\quad s9(+1) \prec s6(-1) \prec s8(-1) \prec s10(-1) \prec s9(+10) \prec s6(-10) \prec s8(-10) \prec s10(-10) \prec [s9(+1),s6(-10),s8(-10),s10(-10)]_f \quad s3(+1)_f$$

$$\text{(C)}\quad s9(+1) \prec s6(-1) \prec s8(-1) \prec s10(-1) \prec [s9(+1),s6(-10),s8(-10),s10(-10)]_f \prec s3(+1)_f$$

Fig. 29. All possible SOOs caused by a large positive disturbance in the flow rate of stream 5 in the two-tank system.

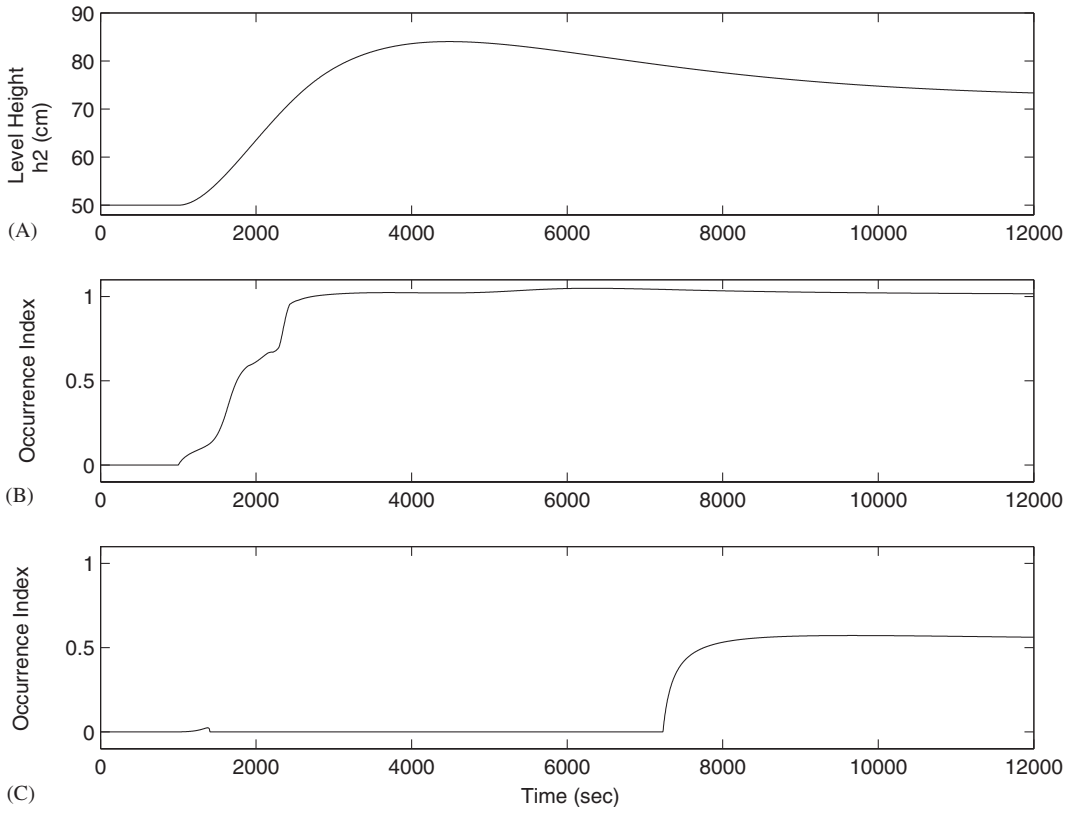

Fig. 30. Diagnosis results using simulation data obtained by introducing a large positive disturbance in the flow rate of stream 4 in the two-tank system described in Fig. 26: (A) dynamic response of liquid level in the second tank; (B) occurrence index of the correct fault origin and (C) occurrence index of the wrong fault origin, i.e., a large positive disturbance in the flow rate of stream 5.

The SOO of a moderate decrease in $m2$ can be obtained by directly applying the construction rules. The two branches in this tree-shaped SOO can be expressed as

$$s7(-1) \prec s5^{(1)}(+1) \prec \cdots \prec [s5(0), s6(-1), s7(-1), s8(-1)]_f, \tag{18}$$

$$s7(-1) \prec s6(-1) \prec s8(-1) \prec s5^{(2)}(-1) \prec \cdots \prec [s5(0), s6(-1), s7(-1), s8(-1)]_f. \tag{19}$$

The corresponding candidate patterns can be obtained by applying the pattern generation algorithms with the override rule outlined in Section 4.1.1. On the other hand, if the propagation time around the feedback loop $m2 \rightarrow h \rightarrow m2$ is shorter than that along the second path of feed forward loop, the above SOO can be simplified by replacing Eq. (19) with

$$s7(-1) \prec s6(-1) \prec s8(-1). \tag{20}$$

Finally, if the disturbance propagation times along the two separate paths of feed forward loop can be assumed to be almost identical, then the branches in Eqs. (18) and (19) can be combined to form an equivalent single-path SOO:

$$s7(-1) \prec s6(-1) \prec s8(-1) \prec s5(0). \tag{21}$$

Under the same assumption, the SOOs of other disturbances can also be produced with the above approach. For example, the SOOs of $m1(+1)$ and $m3(+1)$ can be, respectively, written as

$$s8(+1) \prec s5(+1) \prec s7(+1) \prec s6(+1) \prec s8(+10) \prec \cdots \prec [s5(+10), s6(+10), s7(+10), s8(+10)]_f, \tag{22}$$

$$s5(+1) \prec s7(+1) \prec s6(+1) \prec s8(+1) \prec s5(+1) \prec \cdots \prec [s5(+10), s6(+10), s7(+10), s8(+10)]_f. \tag{23}$$

Notice that the final nodes of the SOOs in these two equations are identical. If the IF–THEN rules are constructed according to the procedure previously described in Section 2, it is clear that the resulting FIS is incapable of distinguishing the corresponding fault origins. On the other hand, it should be noted that the initial nodes of these two SOOs are arranged differently. This observation implies that the diagnostic resolution of a FIS may be further enhanced by incorporating the historical records of on-line symptoms into the inference mechanism. This improved inference structure is presented in detail in the following section.

5. Two-layer inference structure

As mentioned previously, the total number of possible candidate patterns N_{CP} can be computed easily with Eqs. (2)–(4).

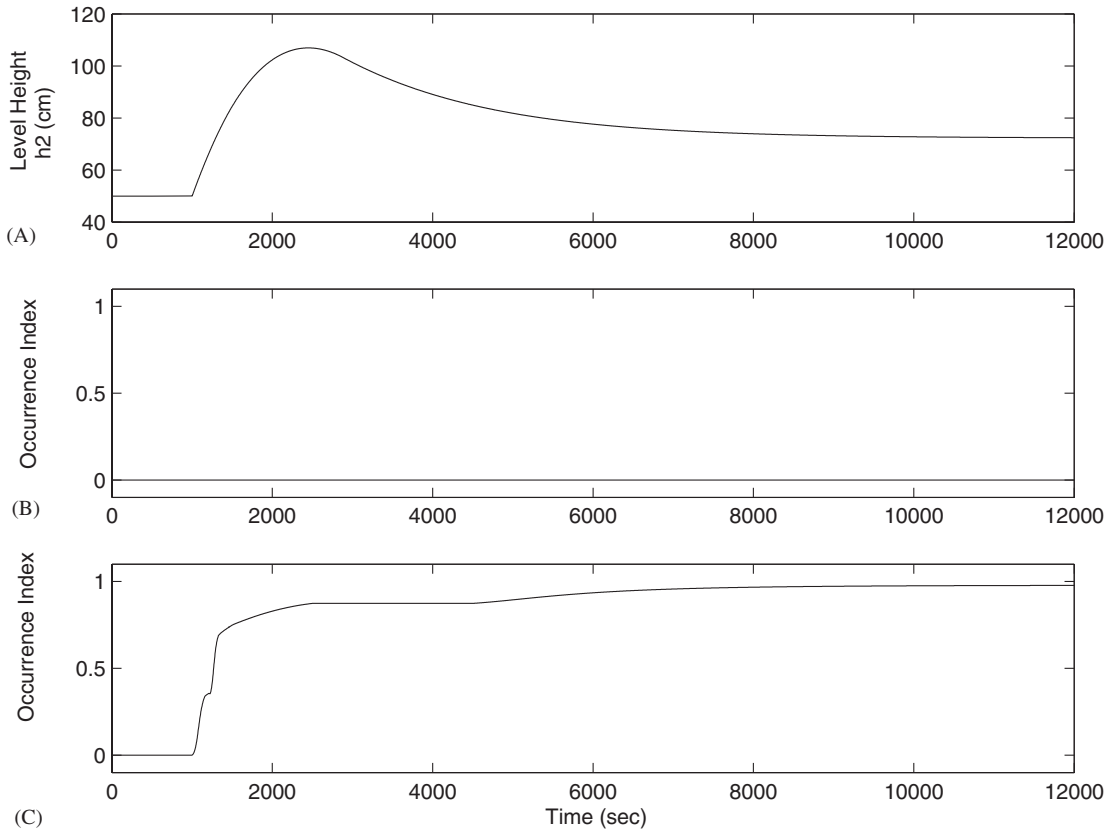

Fig. 31. Diagnosis results using simulation data obtained by introducing a large positive disturbance in the flow rate of stream 5 in the two-tank system described in Fig. 26: (A) dynamic response of liquid level in the second tank; (B) occurrence index of the wrong fault origin, i.e., a large positive disturbance in the flow rate of stream 4; and (C) occurrence index of the correct fault origin.

It should be understood that some of these patterns may not show up in a realistic application and, also, the rest observable patterns must appear one-by-one in a definite sequence. Let us again consider the level control system in Fig. 2 as an example. The SOO of cust set 9 and the corresponding candidate patterns can be found in Fig. 5(B) and Table 2, respectively. It should be noted that, other than the structure of SOO, the numbers of *occurred* symptoms in these patterns can also be used as the basis for determining their occurrence order in time. More specifically, the fewer the number of occurred symptoms included in a pattern the earlier it can be observed on-line. Thus, it can be deduced that the basic events in cut set 9 can result in *only one* of the following three sequences of symptom patterns:

$$\mathbf{PES}_1 : 1 \prec 2 \prec 3 \prec 5 \prec 7, \tag{24}$$

$$\mathbf{PES}_2 : 1 \prec 2 \prec 4 \prec 5 \prec 7, \tag{25}$$

$$\mathbf{PES}_3 : 1 \prec 2 \prec 4 \prec 6 \prec 7. \tag{26}$$

Notice that every pattern in the above equations is represented with a numerical label and the corresponding symptoms can be found in Table 2. Each series of patterns is referred to in this paper as a *pattern evolution sequence* (PES).

The task of fault diagnosis can be viewed as that of identifying a match between the historical record of on-line symptoms and one of the PESs. In our study, a two-layer inference structure is used for this purpose. The first layer is used for comparing the *current* on-line symptoms with every individual candidate pattern, and then generating a measure of agreement between them. More specifically, let us consider the inference rules given in Table 3. These rules, which are originally used for evaluating the occurrence index associated with cut set 9, can be converted to those used for computing the *agreement measures* of seven candidate patterns (say $p1$–$p7$), respectively. The maximum values of these measures, $p1^m, p2^m, \ldots, p7^m$, and their respective occurrence times, $t1^m, t2^m, \ldots, t7^m$, are updated every time a new batch of current measurements are taken. Notice that the occurrence times of the maximum agreement measures must be consistent with the precedence order given in one of the PESs. For example, if Eq. (26) is the correct PES for cut set 9, then the following inequality constraint must be satisfied

$$t1^m \leqslant t2^m \leqslant t4^m \leqslant t6^m \leqslant t7^m. \tag{27}$$

If, at any time, this constraint is violated, the outputs of the first-layer inference system, i.e., $p1^m$–$p7^m$, should all be reset to zero.

The second-layer inference system is used for comparing the time profile of on-line measurement data with each PES, and then generating a measure of closeness between these two trends. The inference rules for computing this measure can be

constructed on the basis of the outputs obtained from the first layer. For example, let us consider the fourth pattern in Eq. (26), i.e., pattern 6 in Table 2. The corresponding *closeness measure* $sq3$ can be obtained with the rules given in Table 10. Notice that the rationale for adopting rule 1 in this table is essentially the same as that for rule 6 in Table 2. On the other hand, the remaining rules in Table 10 are used to reduce the closeness measure under the condition that one or more previous pattern in PES is missing. It should be stressed that all other second-layer inference rules for the PESs in Eqs. (24)–(26) can be synthesized with the same approach. A complete listing is omitted here for the sake of conciseness.

Finally, it should be noted that the occurrence index of a fault origin can be determined by taking the largest value among all closeness measures. In the case of cut set 9, this value is

$$\mathrm{cs}_9 = \max\{sq1, sq2, sq3\}. \tag{28}$$

Example 1. To demonstrate the effectiveness of this two-layer inference mechanism, let us consider the fault diagnosis problems in the feed-forward level-control system presented in Fig. 13. Let us assume that the height of tank wall is 100 cm and the outlet flow rate is proportional to the square root of liquid-level height. To carry out numerical simulation studies, it is also assumed that the system is initially at the normal steady state when the level height is 50 cm and the flow rates of both streams 1 and 2 are the same (707 cm^3/s). The valve on stream 3 is normally kept closed at any time. Finally, a proportional controller is used to implement the feed forward strategy and its gain is chosen to be 0.07. The effects of two different fault origins, i.e., $m1(+1)$ and $m3(+1)$, have been simulated numerically in this example. The disturbance propagation scenario in the former case was simulated by increasing the flow rate of stream 1 from its normal level to 849 cm^3/s at 1500 s. The latter scenario can be considered as the result of mistakenly opening valve V-03. The corresponding simulation run was performed by introducing an additional input flow rate of 200 cm^3/s to the tank at 1500 s. The time profiles of the measured process variables, i.e., input flow rate ($m1$), output flow rate ($m2$) and level height (h), and also the controller output ($s6$) in these two cases are plotted in Figs. 15(A)–(D) and 16(A)–(D), respectively. As mentioned previously, the fault origins considered in this example cannot really be distinguished with the one-layer inference scheme. Indeed, this prediction can be confirmed in the simulation results of the corresponding occurrence indices presented in Figs. 15(E), (F), 16(E) and (F). On the other hand, the diagnostic resolution can be much improved by adopting the two-layer inference structure, which is quite evident in Figs. 17 and 18. This improvement is achieved by identifying the two distinct PESs associated with Eqs. (22) and (23). In particular, notice that a significant increase in the input flow rate $m1$ occurs much earlier in Fig. 15(A) than in Fig. 16(A).

6. Case studies

To demonstrate the effectiveness of the proposed fault diagnosis approach, extensive numerical simulation studies have been carried out in this work. The on-line measurement data of all fault propagation scenarios were generated with SIMULINK (Mathworks, 2002b). These data were then used in inference calculations with the fuzzy-logic module in MATLAB toolbox (Mathworks, 2002a). Three typical examples are presented below.

Example 2. First let us again consider the level control system in Fig. 2. The process parameters used in simulation runs are the same as those adopted in Example 1. A PI controller was used in this case and its parameters were chosen with the IMC design method, i.e., $K_c = 1.4145$ and $\tau_I = 1436.2$. As mentioned previously in subsection 4.1, the basic event "an uncontrollable increase in the flow rate of stream 3" is a possible root cause of system hazard under study, i.e., high liquid level. The corresponding SOOs have already been derived and presented in Fig. 10. Consequently, the fuzzy inference rules can be constructed easily according to the resulting candidate patterns, e.g., see Table 7. The effects of this fault origin were simulated by introducing an additional flow rate of 900 cm^3/s in stream 3 at 1000 s during simulation run. The time profiles of the measured process variables and also the controller output are plotted in Fig. 19. The occurrence index of the event "$m3(+10)$" can be found in Fig. 20(A). It can be observed that the diagnosis is clearly swift and quite accurate. Specifically, the existence of fault origin is detected almost immediately and fully confirmed at about 500 s after its introduction.

On the other hand, it should be noted that the fault propagation scenario associated with cut set 9 was also simulated in this case study by fixing the position of control valve CV-01 at 750 s and then introducing an additional flow rate of 200 cm^3/s in stream 3 at 1000 s. The occurrence index of the assumed fault origin "$m3(+10)$" is presented in Fig. 20(B). Notice that the nonzero occurrence index in the period between 1000 and 2600 s can be attributed to the fact that the candidate patterns of the wrong fault origin in this case are matched partially. However, as the on-line symptoms developed further, none of them can be used to characterize the measurement data obtained after 2600 s and thus the occurrence index drops to zero abruptly.

Example 3. Next, let us consider ratio control system in Fig. 11. The system model and its parameters are given in Appendix A. A PI controller was adopted in this system, and its parameters were chosen to be: $K_{c,1} = 0.02$ and $\tau_{I,1} = 0.2$. In this example, the fault origin under study is the event "a large disturbance in flow A," i.e., $m1(+10)$. The corresponding SOO has already been given in Section 4.2. In the simulation run, the flow rate of reactant A was increased to 5000 cm^3/s at 10 s. The simulation results of the flow-ratio measurement and the corresponding occurrence index are plotted in Figs. 21(A) and (B), respectively. As expected, the diagnosis of the proposed FIS is correct in this case.

A second ratio control system has also been studied in this example. As shown in Fig. 22, it is configured by adding another feedback loop in the previous system to control the flow rate of input A. The chosen controller parameters were: $K_{c,1} = 0.002$,

$\tau_{I,1} = 0.2$, $K_{c,2} = 0.0002$ and $\tau_{I,2} = 0.2$. The corresponding digraph model can be found in Fig. 23. The fault origin considered in this case is a sensor bias in the flow measurement data of stream A. This failure is in fact one of the root causes of system hazard, i.e., a decrease in the flow ratio B/A. The resulting SOO is presented in Fig. 24 and it was derived according to the techniques given in Section 4. The effectiveness of the fuzzy diagnosis rules can be again verified with the simulation results shown in Fig. 25.

Example 4. Finally, let us consider the two-tank system presented in Fig. 26. The system model and parameters are presented in Appendix B. Notice that, in this system, the height of liquid level in the second tank is controlled with a PI controller by manipulating the input flow of the first tank. Again the IMC design method was used to determine the controller parameters. The selected parameter values are: $K_c = 1.4195$ and $\tau_I = 2578.5$. The digraph of this system is shown in Fig. 27.

Two different fault origins have been studied, i.e., (1) a large positive disturbance in stream 4 and (2) a large positive disturbance in stream 5. Both events lead to the eventual increase of the liquid level in tank 2. In order to simplify the SOOs and thus the inference logics, the disturbance propagation time from every state variable to its on-line measurement signal, e.g., from $h1$ to $s10$, is assumed to be negligible. For the same reason, it is also assumed that the output flow rate of each tank responds almost immediately to a change in the corresponding liquid level, e.g., $q2$ reacts instantaneously to any variation in $h1$. On the basis of these assumptions, the possible SOOs resulting from the above two fault origins can be derived with the proposed procedure (see Figs. 28 and 29).

To simulate the first scenario, the flow rate of stream 4 was increased to $850\,\mathrm{cm}^3/\mathrm{s}$ at 1000 s. In a separate simulation run, the flow rate of stream 5 was raised to $850\,\mathrm{cm}^3/\mathrm{s}$ at 1000 s instead. The corresponding diagnosis results are presented in Figs. 30 and 31, respectively. It can be observed that the diagnosis is done very quickly and also quite accurate not only in identifying the correct fault origins but also in rejecting the wrong ones. Also, notice that the occurrence index of the wrong fault origin in the first scenario reaches approximately 0.6 after 8000 s [Fig. 30(C)]. This phenomenon can be explained by comparing data taken at any instance in this period with the membership functions used in the inference rules for diagnosing the wrong origin. It was found that the corresponding candidate patterns were in fact partially matched.

Finally, it can be determined that approximately 4.2×10^{-5} s is needed on an AMD Athlon (tm) XP2400 PC (2.00 GHz) to produce a new occurrence index associated with the fault origin $m4(+10)$, while 5.4×10^{-5} was needed for $m5(+10)$. The numbers of IF–THEN rules used in the FIS were 102 and 164 for these two origins, respectively. Since the total number of cut sets considered in this system is only 14, it is obvious that all corresponding occurrence indices can be easily computed at very short time intervals and, thus, the on-line computation resources required to implement the proposed strategy are relatively modest.

7. Conclusions

The complex fault propagation behaviors in practical process systems are characterized qualitatively in this study with fuzzy IF–THEN rules. To facilitate formulation of these rules, a series of systematic procedures have been developed to produce the occurrence orders, candidate patterns and patterns evolution sequences of the on-line symptoms. A two-layer inference system can then be assembled accordingly for fault diagnosis purpose. From the numerical simulation results presented in this paper, it is obvious that the proposed approach is quite effective in enhancing the diagnostic resolution. Furthermore, this inference scheme can be used not only to identify the correct fault origins but also to confirm the corresponding fault propagation mechanisms as well.

Notation

aia1, aia2	sudden variations in the instrument air pressure supply to the electric/pneumatic signal converter FY1 and FY2, respectively
atd1, atd2	sensor failures (i.e., a drift in the zero) corresponding to FT1 and FT2, respectively
bcvfc1, bcvfc2	control valves 1 and 2 failing close, respectively
bfd3	a hardware failure causing abnormal deviation in the output of ratio station FY3
btd1, btd2	the hardware failures of sensor FT1 and FT2, respectively
cs1	controller FIC1 stuck
cs_k	the occurrence index of kth cut set
CV-01, CV-02	labels of control valves 1 and 2, respectively
cvs1	the control valve 1 stuck
F	the linguistic interpretation function
FIC	flow indicator controller
FT	flow transmitter
FY	electric/pneumatic signal converter
LN	"large negative"—a linguistic value of the normalized process deviation
LIC	level indicator controller
LP	"large positive"—a linguistic value of the normalized process deviation
m_i	the mass flow rate in pipeline i
$\mathcal{N}\{\cdot\}$	counting operator in computing total number of candidate patterns
N_{CP}	the number of candidate patterns
NOC	"not occurred"—a linguistic value of the occurrence index
OCR	"occurred"—a linguistic value of the occurrence index
$\mathbf{P}^{(0)}(n_0)$	the initial path of length n_0
$\mathbf{P}^{(0,i)}(n_{0,i})$	the ith branch path from $\mathbf{P}^{(0)}$ of length $n_{0,i}$
$\mathbf{P}^{(0,i,j)}(n_{0,i,j})$	the jth branch path of length $n_{0,i,j}$

pi^m	the maximum agreement measure of the ith candidate pattern
r	flow ratio
rm	flow-ratio measurement
s_i	the electric or pneumatic signals in lines i
SN	"small negative"—a linguistic value of the normalized process deviation
SP	"small positive"—a linguistic value of the normalized process deviation
sp	set point of controller
T-01	tank number 1
ti^m	the occurrence time of pi^m
$tr2$	the sensor FT2
$trs1$	the sensor FT1 stuck
UCT_i	uncertain with confidence degree i—a linguistic value of the occurrence index
V-02, V-03	labels of valve 2 and 3
ZE	"zero"—a linguistic value the normalized process deviation

Greek letters

δ_j	the qualitative deviation value of process variable j

Acknowledgements

This work is supported by the National Science Council of the ROC government under Grant NSC93-2214-E-006-016.

Appendix A. Dynamic model of ratio control systems

Table A.1 shows the model variables and parameters of the ratio control systems.

- *Chemical reaction*:

$$A + B \rightarrow C. \tag{A.1}$$

- *Reaction rate*:

$$\bar{r} = k\mathrm{e}^{(-E/RT)} C_A C_B^{-1}. \tag{A.2}$$

- *Mass balances*:

$$A\frac{\mathrm{d}h}{\mathrm{d}t} = q_A + q_B - q_5, \tag{A.3}$$

$$V\frac{\mathrm{d}C_A}{\mathrm{d}t} = q_A C_{A,0} - q_5 C_A - \bar{r}V, \tag{A.4}$$

$$V\frac{\mathrm{d}C_B}{\mathrm{d}t} = q_B C_{B,0} - q_5 C_B - \bar{r}V, \tag{A.5}$$

$$V\frac{\mathrm{d}C_C}{\mathrm{d}t} = -q_5 C_C + \bar{r}V. \tag{A.6}$$

- *Energy balance*:

$$\frac{\mathrm{d}T}{\mathrm{d}t} = \frac{\dot{Q} + q_A C_A \widetilde{C}_{p,A}(T_A - T) + q_B C_B \widetilde{C}_{p,B}(T_B - T) - \Delta H V \bar{r}}{V(C_A \widetilde{C}_{p,A} + C_B \widetilde{C}_{p,B} + C_C \widetilde{C}_{p,C})}. \tag{A.7}$$

Table A1
Model variables and parameters of the ratio control systems

Variable/parameter	Definition	(Initial) Value
q_5	Flow rate of the reactor output stream	$3150\,\mathrm{cm}^3/\mathrm{s}$
q_A	Flow rate of input stream A	$2100\,\mathrm{cm}^3/\mathrm{s}$
q_B	Flow rate of input stream B	$1050\,\mathrm{cm}^3/\mathrm{s}$
C_A	Concentration of reactant A in reactor	$0.4\,\mathrm{mol/cm}^3$
C_B	Concentration of reactant B in reactor	$0.2\,\mathrm{mol/cm}^3$
C_C	Concentration of product C in reactor	$0.0667\,\mathrm{mol/cm}^3$
$C_{A,0}$	Concentration of reactant A in input stream A	$0.7\,\mathrm{mol/cm}^3$
$C_{B,0}$	Concentration of reactant B in input stream B	$0.8\,\mathrm{mol/cm}^3$
h	Height of liquid level in reactor	100 cm
A	Cross-sectional area of reactor	$10^6\,\mathrm{cm}^2$
ΔH	Heat of reaction	$-3 \times 10^6\,\mathrm{J/mol}$
$\widetilde{C}_{p,A}$	Average heat capacity of reactant A	40 J/mol K
$\widetilde{C}_{p,B}$	Average heat capacity of reactant B	30 J/mol K
$\widetilde{C}_{p,C}$	Average heat capacity of product C	25 J/mol K
T_A	Temperature of input stream A	398.5 K
T_B	Temperature of input stream B	398.5 K
T	Reactor temperature	398.5 K
E	Activation energy	14 000 J/mol
R	Universal gas constant	8.314 J/mol K
k	Frequency factor	$7.1837 \times 10^{-4}\,\mathrm{mol/s\,cm}^3$
cv_1	Control valve gain on stream B	$21\,\mathrm{cm}^3/\mathrm{s}\%$
FY_1	Desired feed ratio value	0.5
$\dot{Q}$	External heat supply rate	$-6.3 \times 10^8\,\mathrm{J/s}$
cv_2	Control valve gain on stream A	$42\,\mathrm{cm}^3/\mathrm{s}\%$
$q_{A,\mathrm{set}}$	Set point of flow controller on stream A	$2100\,\mathrm{cm}^3/\mathrm{s}$

Table B1
Model variables and parameters of the two-tank system

Variable/parameter	Definition	(Initial) Value
A_1	Cross-sectional area of tank 1	$2 \times 10^4\,\mathrm{cm}^2/\mathrm{s}$
h_1	Height of liquid level in tank 1	$29.59\,\mathrm{cm}^2/\mathrm{s}$
A_2	Cross-sectional area of tank 2	$10^4\,\mathrm{cm}^2/\mathrm{s}$
h_2	Height of liquid level in tank 2	50 cm
q_1	Input flow rate of tank 1	$707.11\,\mathrm{cm}^3/\mathrm{s}$
q_2	Output flow rate of tank 1	$707.11\,\mathrm{cm}^3/\mathrm{s}$
q_3	Output flow rate of tank 2	$707.11\,\mathrm{cm}^3/\mathrm{s}$
q_4	Disturbance flow rate to tank 1	$0\,\mathrm{cm}^3/\mathrm{s}$
q_5	Disturbance flow rate to tank 2	$0\,\mathrm{cm}^3/\mathrm{s}$
C_1	Proportional constant in flow model of q_2	$130\,\mathrm{cm}^{2.5}/\mathrm{s}$
C_2	Proportional constant in flow model of q_3	$100\,\mathrm{cm}^{2.5}/\mathrm{s}$
cv	Control valve gain	$15\,\mathrm{cm}^3/\mathrm{s}\%$
h_{set}	Set point of level controller	50 cm

- *Control laws*:

$$q_B = \mathrm{cv}_1 K_{c,1}\left[(q_A F Y_1 - q_B) + \frac{1}{\tau_{I,1}}\int_0^t (q_A F Y_1 - q_B)\right], \tag{A.8}$$

$$q_A = \mathrm{cv}_2 K_{c,2}\left[(q_{A,\mathrm{set}} - q_A) + \frac{1}{\tau_{I,2}}\int_0^t (q_{A,\mathrm{set}} - q_A)\right]. \tag{A.9}$$

Appendix B. Dynamic model of two-tank system

Table B.1 shows the model variables of the two-tank system.

- *Mass balances*:

$$A_1\frac{\mathrm{d}h_1}{\mathrm{d}t} = q_1 + q_4 - q_2, \tag{B.1}$$

$$A_2\frac{\mathrm{d}h_2}{\mathrm{d}t} = q_2 + q_5 - q_3. \tag{B.2}$$

- *Flow models*:

$$q_2 = C_1\sqrt{h_1}, \tag{B.3}$$

$$q_3 = C_2\sqrt{h_2}, \tag{B.4}$$

- *Control law*:

$$q_1 = \mathrm{cv}K_c\left[(h_{\mathrm{set}} - h_2) + \frac{1}{\tau_I}\int_0^t (h_{\mathrm{set}} - h_2)\right]. \tag{B.5}$$

References

Allen, D.J., 1984. Digraphs and fault trees. I&EC Fundamentals 23, 175.

Allen, D.J., Rao, M.S.M., 1980. New algorithms for the synthesis and analysis of fault trees. I&EC Fundamentals 19, 79.

Andrews, J.D., Brennan, G., 1990. Application of the digraph method of fault tree construction to a complex control configuration. Reliability Engineering and System Safety 28, 357.

Andrews, J.D., Morgan, J.M., 1986. Application of digraph method of fault tree construction to process plant. Reliability Engineering 14, 85.

Bakshi, B.R., Stephanopoulos, G., 1994a. Representation of process trends—III: multiscale extraction of trends from process data. Computer and Chemical Engineering 18, 267.

Bakshi, B.R., Stephanopoulos, G., 1994b. Representation of process trends—IV: induction of real-time patterns from operating data for diagnosis and supervisory control. Computer and Chemical Engineering 18, 303.

Chamow, M.F., 1978. Directed graph techniques for the analysis of fault trees. IEEE Transactions on Reliability R-27, 7.

Chang, S.Y., Chang, C.T., 2003. A fuzzy-logic based fault diagnosis strategy for process control loops. Chemical Engineering Science 58, 3395.

Chang, C.T., Chen, J.W., 1995. Implementation issues concerning the ekf-based fault diagnosis technique. Chemical Engineering Science 50, 2861.

Chang, C.T., Hwang, H.C., 1992. New developments of the digraph-based techniques for fault-tree synthesis. Industrial & Engineering Chemistry Research 31, 1490.

Chang, C.T., Hwang, K.S., 1994. Studies on the digraph-based approach for fault-tree synthesis, 1: the ratio-control systems. Industrial & Engineering Chemistry Research 33, 1520.

Chang, C.T., Hsu, D.S., Hwang, D.M., 1994. Studies on the digraph-based approach for fault-tree synthesis, 2: the trip systems. Industrial & Engineering Chemistry Research 33, 1700.

Chang, S.Y., Lin, C.R., Chang, C.T., 2002. A fuzzy diagnosis approach using dynamic fault trees. Chemical Engineering Science 57, 2971.

Cummings, D.L., Lapp, S.A., Powers, G.J., 1983. Fault tree synthesis from a directed graph model for a power distribution network. IEEE Transactions on Reliability R-32, 140.

Dash, S., Rengaswamy, R., Venkatasubramanian, V., 2003. Fuzzy-logic based trend classification for fault diagnosis of chemical process. Computer and Chemical Engineering 27, 347.

Horowitz, E., Sahni, S., 1984. Fundamentals of DATA STRUCTURE IN PASCAL. Computer Science Press, Rockville, MD.

Hoskins, J.C., Kalivur, K.M., Himmeblau, D.M., 1991. Fault diagnosis in complex chemical-plants using artificial neural networks. A.I.Ch.E. Journal 37, 137.

Iri, M., Aoki, K., O'Shima, E., Matsuyama, H., 1979. An algorithm for diagnosis of system failure in the chemical process. Computer and Chemical Engineering 3, 489.

Ju, S.N., Chen, C.L., Chang, C.T., 2003. Fault tree structures of override control systems. Reliability Engineering System Safety 81, 163.

Ju, S.N., Chen, C.L., Chang, C.T., 2004. Constructing fault trees for the advanced process control systems—an application to the cascade control loops. IEEE Transactions on Reliability 53, 43.

Kramer, M.A., Palowitch Jr, B.L., 1987. A rule-based approach to fault diagnosis using the signed directed graph. A.I.Ch.E. Journal 33, 1067.

Kuipers, B.J., 1994. Qualitative Reasoning: Modeling and Simulation with Incomplete Knowledge. MIT Press, Cambridge, MA.

Lambert, H.E., 1979. Comments on the Lapp–Powers 'Computer-aided synthesis of fault trees'. IEEE Transactions on Reliability R-28, 6.

Lapp, S.A., Powers, G.J., 1977. Computer-aided synthesis of fault trees. IEEE Transactions on Reliability R-26, 2.

Lapp, S.A., Powers, G.J., 1979. Update of Lapp–Powers fault-tree synthesis algorithm. IEEE Transactions on Reliability R-28, 12.

Lu, N., Wang, F., Gao, F., 2003. Combination method of principal component and wavelet analysis for multivariate process monitoring and fault diagnosis. Industrial & Engineering Chemistry Research 42, 4198.

Mathworks, 2002a. Fuzzy Logic Toolbox-User Guide. The Mathworks Inc., Natick, MA.

Mathworks, 2002b. SIMULINK—Dynamic System Simulation for MATLAB-Using Simulink. The Mathworks Inc., Natick, MA.

Maurya, M.R., Rengaswamy, R., Venkatasubramanian, V., 2004. Application of signed digraph-based analysis for fault diagnosis chemical process flowsheets. Engineering Applications of Artificial Intelligence 17, 501.

Petti, T.F., Klein, J., Dhurjati, P.S., 1990. Diagnostic model processor: using deep knowledge for process fault dianosis. A.I.Ch.E. Journal 36, 565.

Shaeiwitz, J.A., Lapp, S.A., Powers, G.J., 1977. Fault tree analysis of sequential systems. I&EC Proceedings Design and Development 16, 529.

Shiozaki, J., Matuyama, H., O'Shima, E., Iri, M., 1985. An improved algorithm for diagnosis of system failures in the chemical process. Computer and Chemical Engineering 9, 285.

Tarifa, E.E., Scenna, N.J., 2004. Fault diagnosis for MSF dynamic states using a SDG and fuzzy logic. Desalination 166, 93.

Tsunge, Y., Shiozaki, J., Matuyama, H., O'Shima, E., 1985. Fault diagnosis algorithms based on the signed directed graph and its modifications. Institute of Chemical Engineering Symposium Series 92, 133.

Ulerich, N.H., Powers, G.J., 1988. Online hazard aversion and fault diagnosis in chemical processes: the digraph + fault-tree method. IEEE Transactions on Reliability 37, 171.

Zhang, Z.Q., Wu, C.G., Zhang, B.K., Xia, T., Li, A.F., 2005. SDG multiple fault diagnosis by real-time inverse inference. Reliability Engineering System Safety 87, 173.